Blob structure and motion in the edge and SOL of NSTX

2016 Plasma Phys. Control. Fusion 58 044007

(http://iopscience.iop.org/0741-3335/58/4/044007)

IOP Publishing Plasma Physics and Controlled Fusion

Plasma Phys. Control. Fusion **58** (2016) 044007 (18pp) doi:10.1088/0741-3335/58/4/044007

Blob structure and motion in the edge and SOL of NSTX

S J Zweben[1], J R Myra[2], W M Davis[1], D A D'Ippolito[2], T K Gray[3], S M Kaye[1], B P LeBlanc[1], R J Maqueda[1,4], D A Russell[2], D P Stotler[1] and the NSTX-U Team

[1] Princeton Plasma Physics Laboratory, Princeton, NJ 08540 USA
[2] Lodestar Research Corporation, Boulder, CO 80301, USA
[3] Oak Ridge National Laboratory, Oak Ridge, TN 37831, USA

E-mail: szweben@pppl.gov

Received 6 October 2015, revised 4 December 2015
Accepted for publication 16 December 2015
Published 28 January 2016

Abstract

The structure and motion of discrete plasma blobs (a.k.a. filaments) in the edge and scrape-off layer of NSTX is studied for representative Ohmic and H-mode discharges. Individual blobs were tracked in the 2D radial versus poloidal plane using data from the gas puff imaging diagnostic taken at 400 000 frames s^{-1}. A database of blob amplitude, size, ellipticity, tilt, and velocity was obtained for ~45 000 individual blobs. Empirical relationships between various properties are described, e.g. blob speed versus amplitude and blob tilt versus ellipticity. The blob velocities are also compared with analytic models.

Keywords: tokamak, turbulence, edge

(Some figures may appear in colour only in the online journal)

1. Introduction

The goal of this paper is to describe the structure and motion of the plasma blobs in the edge and scrape-off-layer (SOL) of the NSTX spherical tokamak. Plasma 'blobs' are relatively isolated structures which are formed in the plasma edge or near the magnetic separatrix, and move radially into the SOL (sometimes called 'filaments', 'bursts', or 'intermittent plasma objects'). The present measurements were made using a 2D gas puff imaging (GPI) diagnostic, and compared with analytic models for blob velocity. For the sake of simplicity and clarity we focus on two specific plasma conditions: one Ohmic and one H-mode, using GPI data from seven nearly-identical shots in each case. These results are relevant for understanding the cross-field transport in the SOL of tokamaks, and for future comparisons of edge turbulence measurements with modeling of the SOL, e.g. for ITER.

The central concept of the outward convective motion of an isolated blob in the SOL of a tokamak was proposed by Krasheninnikov in 2001 [1], and since then there have been many refinements of the analytic theory of blob structure and motion, as described in the review papers [2, 3]. Recent computational studies of blobs have shown that the expected structure and motion of blobs can become quite complicated, depending on the details of tokamak geometry [4, 5], the regime of collisionality [2, 3, 6, 7], inclusion of ion temperature effects [8–10], drift wave and other 3D effects [11–13], kinetic effects [14–16], and density gradients [17, 18]. Even the relationship between simplified analytic blob models and the results of computational simulations is not always clear, since the analytic models generally do not describe the blob formation process or blob–blob interactions. Some recent models describe blobs only in a statistical sense [19–21].

Given the complexity of blob theory and the difficulty of blob measurements in tokamaks, it is not surprising that the connection between blob experiments and theory is imprecise and incomplete. A review in 2011 [3] plotted the dimensionless blob sizes and radial velocities for nine tokamaks versus two analytic blob models (sheath-connected and inertial regimes), and showed that most of the data points fell between these two scalings, but with considerable uncertainty and scatter. More recently, agreement of radial blob velocities at about the 50% level with a warm ion model could be obtained for

[4] Currently at: X Science LLC, Plainsboro, NJ 08536, USA.

selected discharges on ASDEX-Upgrade [22]. In a different set of experiments, a regime transition for blob dynamics was correlated with collisionality in the MAST divertor [5], and clearer comparisons have been obtained for blobs in simpler magnetic geometries, such as Torpex [23] and VTF [24].

The present paper builds on several previous experimental and theoretical studies of blobs in NSTX. The initial GPI results using He I line emission showed a broad spread of blob velocity in both radial and poloidal directions, with a radial velocity roughly independent of blob amplitude [25]. An early theoretical comparison [26] focused on a small set of blobs in L-mode and H-mode shots, and showed that their radial motion was bounded by the minimum and maximum speeds predicted from analytic blob models. Subsequently, a reduced 2D edge turbulence simulation was made using the SOLT code [27], and initial results were compared with fluctuation levels, blob structure, and heat flux SOL width measurements. A synthetic GPI diagnostic was added to SOLT [28] and further comparisons with GPI were made, including a sensitivity study with respect to various theoretical assumptions. Intermittent blob-filaments were observed using Li I light emission near the lower divertor plates in NSTX [29], and were highly correlated with midplane blobs measured by GPI. The intermittency in the SOL during H-modes was studied at neutral beam power levels from $P_{NBI} = 0$–6 MW, showing the lowest blob activity in Ohmic H-modes and low blob activity shortly after L–H transitions [30]. Recent SOLT simulations and GPI data were compared with respect to the effect of edge sheared flows on blobs, and detailed GPI blob tracking for one NSTX shot was interpreted in terms of edge shear flows [31]. A set of Langmuir probe measurements in NSTX showed intermittent SOL structures with a radial size ~5–10 cm and outward velocity ~3–5 km s^{-1}, roughly consistent with GPI measurements, along with inward propagating voids inside the separatrix [32]. Most recently, the variations of edge turbulence and blobs over a large NSTX GPI database was described [33]. However, that paper discussed only the average behavior of blobs in each shot (including the shots used in the present paper), but did not describe the individual blob behavior or the statistical distribution of blobs within a given type of shot, which is the focus of the present paper.

The outline of this paper is as follows: section 2 describes the plasma parameters for the shots used in this experiment, section 3 describes the theoretical blob regimes, section 4 describes the blob diagnostics and data analysis, and section 5 gives an overall comparison of the blobs between Ohmic and H-mode regimes. Section 6 describes the blob radial velocity, section 7 describes the blob poloidal velocity, and section 8 describes the blob structure. Finally, section 9 discusses blob SOL width, and section 10 contains a summary and discussion.

2. Plasma parameters

Table 1 lists the main parameters for the Ohmic and H-mode discharges used in this paper, evaluated at the time of the GPI gas puff, based on seven nearly identical shots for each case (there were too few L-mode cases for a similar data set). All shots had the same plasma current (830 kA), but the H-mode shots had a slightly higher toroidal field than the Ohmic shots ($B_t = 4.9$ kG versus 3.6 kG), and the H-mode shots had $P_{NBI} = 4$ MW of neutral beam power and higher stored energy ($W = 220$ kJ versus 32 kJ for the Ohmic plasmas). All shots were lower-single-null shape with deuterium fueling, and without any transient events such as ELMs or large MHD during the time of interest. At the bottom of table 1 are edge plasma parameters: the drift-wave gyroradius [10]: $\rho_s = 10^2(M_i T_e)^{1/2}/Z_i B_t$ (where B_t is the toroidal field at the GPI location, $M_i = 2$ and $Z_i = 1$), the electron–ion collision time $\tau_{ei}(=1/\nu_{ei})$, the electron beta β_e, and blob statistics. A similar table was used previously in a paper describing the larger database [33].

Table 1. Parameters for this database.

	Ohmic	H-mode
Shot range	141 746–756	140 389–395
Time range (s)	0.213–0.214	0.535–0.550
I_p (kA)	830	830
B_t (kG)	3.6	4.9
Kappa (elongation)	1.9	2.4
W_{mhd} (kJ)	32	220
n_e average (10^{13} cm^{-3})	1.6	5.2
P_{NBI} (MW)	0	4.0
T_e (0) (eV)	530	920
n_e (0) (10^{13} cm^{-3})	2.3	5.6
T_e (a) (eV)	13 ± 6	29 ± 17
n_e (a) (10^{13} cm^{-3})	0.37 ± 0.23	0.92 ± 0.54
T_e @ −2 cm (eV)	23 ± 4	134 ± 53
n_e @ −2 cm (10^{13} cm^{-3})	0.47 ± 0.17	2.1 ± 0.47
ρ_s (cm) @ −2 cm	0.2	0.3
τ_{ei} (μs) @ −2 cm	0.5	1.5
β_e @ −2 cm	0.0003	0.005
# of blobs identified	28 800	18 800
# of blob trails	2600	820
Blob trail lifetime (μs)	23	36

The edge profiles of T_e and n_e from the Thomson scattering diagnostic at the time of the GPI gas puff are shown in figures 1(a) and (d), averaged over the seven shots of each type. These data are plotted with respect to the EFIT separatrix position (which varied by less than 1 cm within each shot type), and the shot-to-shot standard deviations are shown as error bars. As expected, inside the separatrix (i.e. radius $\leqslant 0$ cm) the T_e and n_e are much higher for the H-mode plasmas, but outside the separatrix the values are more similar, although the uncertainties are large, particularly for H-modes at radii $\geqslant 2$ cm. Figures 1(b) and (e) show the radial gradients dT_e/dr and dn_e/dr derived from spline fits to the T_e and n_e data; these gradients are much larger inside the separatrix than outside, and much larger for H-mode than for Ohmic plasmas. Figures 1(c) and (f) show the T_e and n_e gradient scale lengths (e.g. $T_e/(dT_e/dr)$, with error bars derived from the error bars in figures 1(a) and (d). The gradient scale lengths for H-mode plasma inside the separatrix are near or below those for Ohmic plasmas, but the uncertainties are too large beyond a radius of 2 cm outside the separatrix to give useful scale lengths.

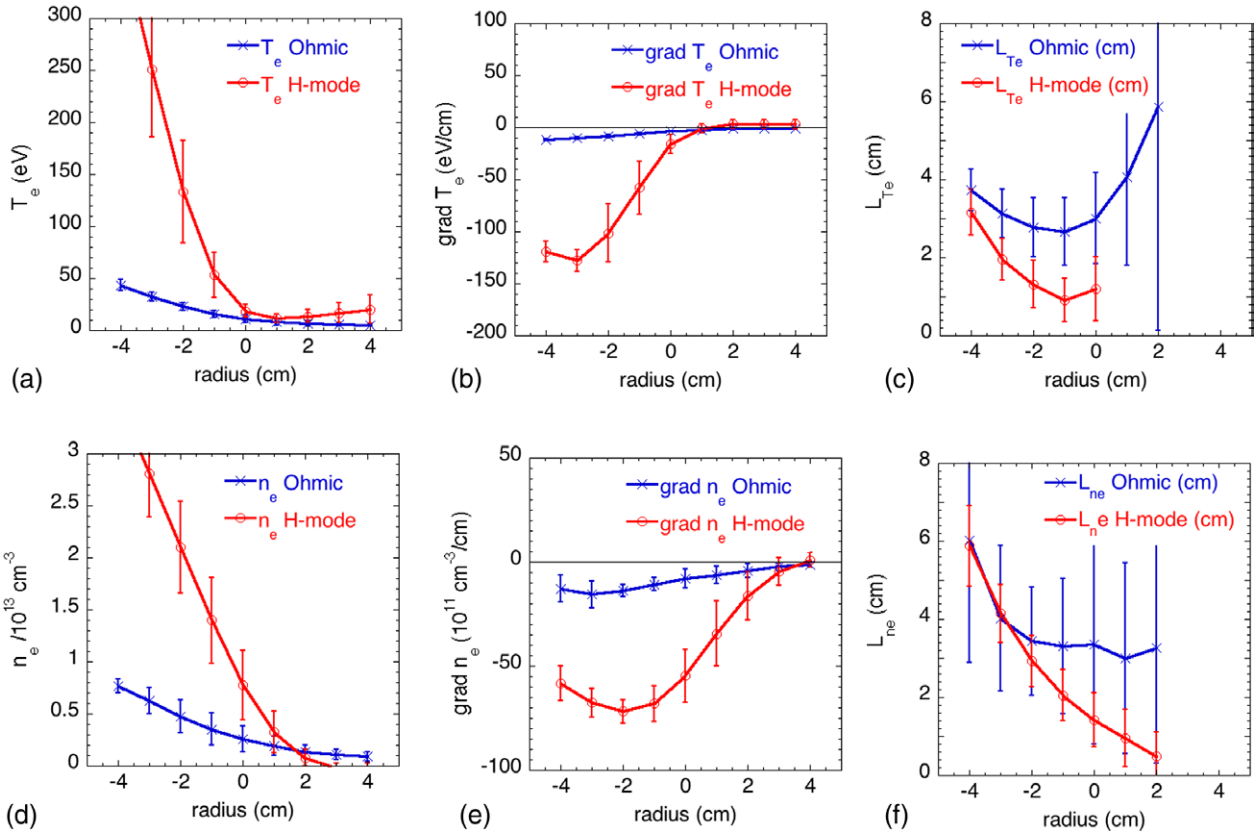

Figure 1. In (a) and (d) are the profiles of n_e and T_e from Thomson scattering for the H-mode and Ohmic discharges in this paper, averaged over the seven shots of each type. In (b) and (e) are the radial gradients of these n_e and T_e profiles, and in (c) and (f) are the radial n_e and T_e scale lengths. The error bars represent the shot-to-shot standard deviations.

3. Blob theory regimes

Based on the plasma parameters of section 2 and the geometry of NSTX, the dimensionless blob theory parameter regimes for these discharges are shown in figure 2. The collision disconnection factor Λ is defined by [3]:

$$\Lambda = \frac{L_{\|}\nu_{ei}}{\rho_s\Omega_e} = 2.75\times 10^{14}\frac{L_{\|}(\mathrm{cm})n_e(\mathrm{cm}^{-3})}{T_e^2(\mathrm{eV})} \qquad (1)$$

and the normalized blob size parameter $\Theta = \widehat{\delta}^{5/2}$, where $\widehat{\delta} = \delta/\delta_*$ and the characteristic blob size parameter is given by:

$$\delta_* = \frac{\rho_s^{4/5}L_{\|}^{2/5}}{R^{1/5}} = 53.4\frac{L_{\|}^{2/5}T_e^{2/5}}{B^{4/5}R^{1/5}}, \qquad (2)$$

where $L_{\|}$ is the parallel connection length along B to the divertor plate ($L_{\|}\sim 500$ cm in the SOL), R is the plasma major radius ($R = 85$ cm), ρ_s is the drift-wave gyroradius, and where the units in the final form of equation (2) are in cm, eV, and Gauss for deuterium plasmas.

The main result in figure 2 is that blobs in this experiment are within a factor of two of the characteristic size where $\widehat{\delta} = 1$. In the far SOL (open circles), blobs in both Ohmic (blue) and H-mode (red) approach the sheath-connected (SC) regime. Near the separatrix (solid circles), the blobs are marginally

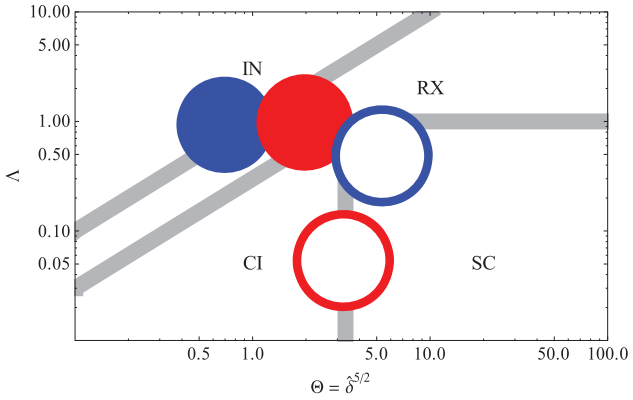

Figure 2. Regime diagram for blob propagation in the parameter space of the collisionality parameter Λ and blob size Θ (see text for definitions). Regimes are: inertial (IN), resistive X-point (RX), sheath connected (SC) and sheath interchange (CI) (see [26] for details). Ohmic (blue) and H-mode (red) data are shown for parameters characteristic of the separatrix ($r = 0$ cm, filled circles) and of the far SOL ($r = 4$ cm, open circles). The size of the circles gives a rough estimate of uncertainties, which are at least a factor of two.

(red for H-mode) or more fully (blue for Ohmic) resistively disconnected from the sheaths, primarily due to higher density and longer connection lengths. But near the separatrix the blobs are also partially in the regimes that are referred to as resistive X-point (RX) or inertial (IN) respectively. It should

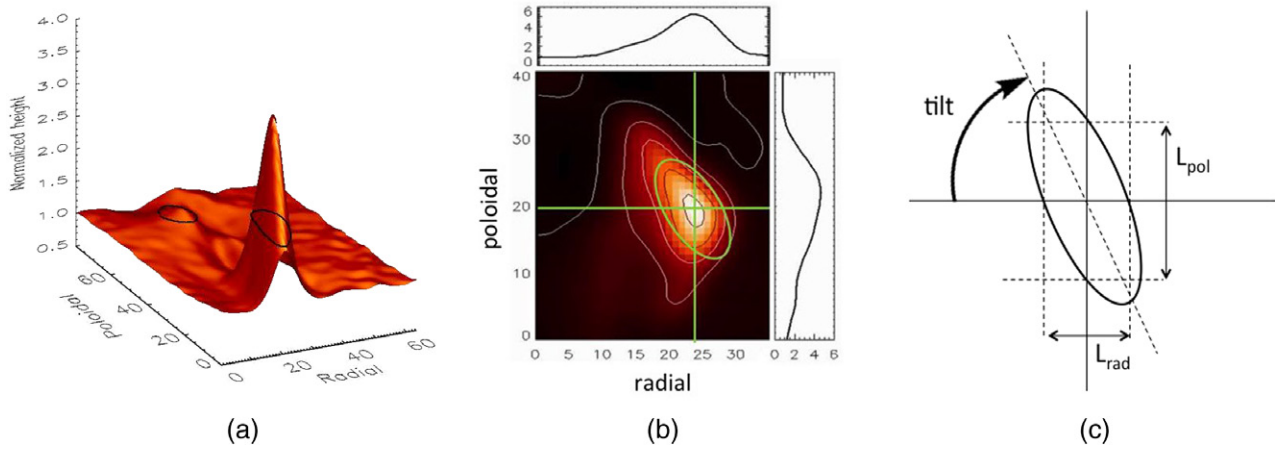

Figure 3. Illustration of the definition of a blob used in this paper. The GPI data are first normalized to a time-averaged image frame, and a blob is defined as the region where the local normalized, smoothed, level becomes ⩾1.5. Contours are generated around each of these regions, and an ellipse is fit to the contour level which is half way between the lowest closed contour (the base of the blob) and the maximum. An example of a normalized frame is shown in (a), typical contours with the ellipse fit (in green) are shown in (b), and blob parameters are defined from the ellipse in (c).

be emphasized that the regime boundaries in figure 2 and the location of the data points are rough estimates with significant (factor of 2 or more) uncertainties. The data points are uncertain due to shot-to-shot standard variations in the density and temperature measurements, and variations in the blob poloidal size $\delta \sim L_{pol}/2$. Furthermore, the mean plasma profiles may differ from actual parameters interior to the blob. The regimes themselves are determined heuristically by balancing various terms in the vorticity equation for charge flow (2) and are thus subject to order unity uncertainties. These heuristic arguments allows scaling estimates for the radial blob velocity to be made in each regime, that transition continuously across regime boundaries. As a result, the IN and sheath-connected (SC) regimes provide useful limiting cases for making comparisons with data (see section 6).

4. Blob diagnostic and data analysis

The NSTX GPI diagnostic used here is the same as described previously [33]. A fast Phantom 710 camera viewed a 30 cm poloidal by 24 cm radial region in the plane perpendicular to the local B field just above the outer midplane near the separatrix. A gas manifold was attached to the nearby wall and puffed deuterium gas into this region, and the D_α light from the neutral deuterium from this puff was viewed through a 657 nm (9 nm FWHM) optical filter at 397 660 frames s^{-1} using an 80 × 64 pixel array. The integration time for each frame was 2.1 μs, the time between frames was 2.5 μs, and the spatial resolution of the optical system was ~0.5 cm at the GPI gas cloud.

Although the GPI data are digitized for ~80 ms per shot, the data in this paper focuses on time periods within ±5 ms of the peak GPI gas puff rate, which includes ~4000 frames (i.e. 40 MB) of data per shot. During this time the GPI signal level is typically 20 times the pre-puff Dα level, yet the perturbation of the gas puff on the edge plasma and edge turbulence was previously found to be negligible [34]. Typical camera signal levels are ~500–1500 counts per pixel in the region of maximum brightness in these 12 bit camera images. As usual in these GPI analyses, no attempt is made to convert the GPI Dα data into local density or temperature fluctuations; the interpretation of the GPI signals in terms of density and temperature was discussed in [33, 34].

The blob tracking analysis of these GPI data was done as follows: all frames are first normalized by a 1 ms rolling time-average of neighboring time frames, in order to identify the relative local maxima in each frame, i.e. the blobs. Such normalization is appropriate since the absolute value of the GPI signals depends on the local neutral density from the GPI gas puff, which is unrelated to the background plasma. A blob is (arbitrarily) defined as a region where the local normalized, smoothed, level becomes ⩾1.5. For example in figure 3(a) the normalized blob height at poloidal position 50 is just above the cutoff of 1.5, and the larger blob at poloidal position 20 is about 4 in normalized height. Contours are then generated around each blob, as illustrated in figure 3(b), and an ellipse (in green) is fit to the contour level half way between the lowest closed contour (the base of the blob) and the local maximum. The location of the blob is defined as the center of these half-maximum ellipse fits, which were then tracked from frame-to-frame along with the ellipticity and tilt angle, as defined in figure 3(c).

The maximum allowed displacement of a given blob between frames was limited to 10 pixels (3.8 cm) to help distinguish different blobs, thus limiting the maximum detectable velocity to 15 km s^{-1}. All blobs were saved in the database if they met these criteria for at least 2 successive frames (5 μs), but ~91% of the blobs in Ohmic plasmas and ~96% of blobs in H-mode plasma were contained in blob trails having a lifetime of ⩾15 μs (6 frames). Note that by this definition a blob can be either inside or outside the separatrix, and that this method does not track negative perturbations ('holes').

Figure 4 shows examples of the blob tracking done for 1 ms of an Ohmic shot (left) and 2 ms of an H-mode shot (right). The start of each blob trail is shown by an ellipse with its initial ellipticity and tilt (but not scaled to size), and each colored

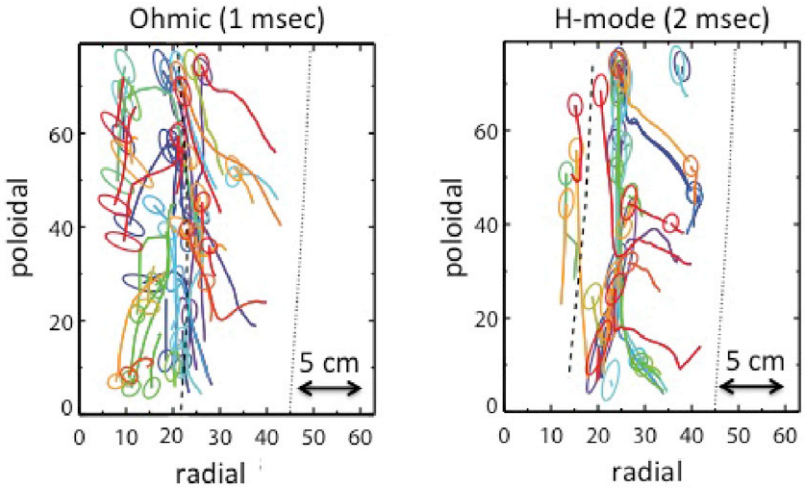

Figure 4. Sample blob trails in the GPI radial versus poloidal plane for an Ohmic shot (left, #141746) and H-mode shot (right, #140395), showing all blobs in a 1 ms period for Ohmic and a 2 ms period for H-mode. The ellipticity and tilt of the initial location of each blob is shown by the ellipses (but the size is not drawn to scale). More blobs are born inside the separatrix (dashed lines) in Ohmic plasmas than in H-mode. The RF limiter shadow is shown by the dotted line.

trail follows a blob until its end (when it fails to meet the above criteria). The average lifetime of these blob trails within the GPI field of view is $\tau_{blob} \sim 23$ μs for the Ohmic cases and $\tau_{blob} \sim 36$ μs for the H-mode cases. The database quantities calculated for each blob for each frame are: the blob center location with respect to the separatrix at that horizontal row, the normalized blob amplitude A_{blob}, the blob ellipticity (major radius/minor radius), the tilt angle (as defined in figure 3), the poloidal and radial sizes of the blobs L_{pol} and L_{rad} (FWHM, as in figure 3), and the poloidal and radial blob velocities V_{pol} and V_{rad}. Here poloidal and radial are approximated as the vertical and horizontal directions in the GPI image frames.

All quantities were evaluated within the 10 ms period near the peak GPI signal, and the blob data was combined into two separate data sets, one for the seven Ohmic shots and one for the seven H-mode shots. The Ohmic data set had ~28 800 individual blobs (counting each blob in each frame), corresponding to ~2600 blob trails like those shown in figure 4(a), and the H-mode data set had ~18 800 blobs with ~820 blob trails like those in figure 4(b).

Figure 5 shows results from the blob database for Ohmic (left, in blue) and H-mode (right, in red), where each point corresponds to a single blob in a single frame. There was no significant difference between the blob results among shots of each type. In figures 5(a) and (b) the blob amplitudes A_{blob} are shown as a function of the distance from the local separatrix; in figures 5(c) and (d) are the corresponding blob V_{rad}, and in figures 5(e) and (f) are the blob $V_{pol.}$ There is a wide spread in these blob properties at each radius, but there are also some systematic variations versus radius over a spatial scale of ~2 cm, to be discussed in section 5.

We reiterate at this point that the analysis in this paper cannot determine the absolute density and/or temperature perturbations in the blobs, and so the blob-induced transport of particles and/or heat cannot be directly evaluated. Thus the implications of these results for the erosion lifetime or heating of first-wall components cannot be assessed with this diagnostic (but see section 9 for an estimate of the SOL width effects).

5. Overall comparison of Ohmic and H-mode blobs

Figure 6 shows an overall comparison of the average blob properties between the Ohmic and H-mode plasmas in this database. The individual blob statistics such as shown in figure 5 have been binned into 2 cm wide radial zones centered between 2 cm inside the separatrix to 6 cm outside the separatrix. Farther inside this region the blobs are entirely within closed flux surfaces, where the simplest definition of a blob [1–3] is not applicable, and farther outside this region there are too few blobs (particularly in Ohmic plasmas), and the GPI signal levels are low. The estimated uncertainty in the radial position as calculated by the EFIT reconstruction is ± 1 cm.

The number of blobs detected per frame per radial zone is clearly different between Ohmic and H-mode cases, as shown in figure 6(a). For Ohmic plasmas the largest number of blobs per zone is found near the separatrix and few blobs were beyond 4 cm outside the separatrix, while in H-mode there were very few blobs inside or near the separatrix, and the number of blobs was nearly constant from 2–6 cm. The small number of blobs detected near the separatrix in H-mode is not related to the ionization of deuterium at larger densities, since the GPI signal level in H-mode is still high between -2 cm and 0 cm [33], but is more related to the relatively low fluctuation level in H-mode inside and near the separatrix [33]. On average, there was ~1 blob/frame in Ohmic plasmas and ~0.5 blob/frame in H-mode plasmas within the radial region of figure 6. Figure 6(b) shows the normalized blob amplitudes, which are between $A_{blob} = 1.5$ (the minimum blob amplitude by definition) and $A_{blob} = 3$ for both types of shots up to 2 cm outside the separatrix, but increase to above 4 at 6 cm for H-mode plasmas.

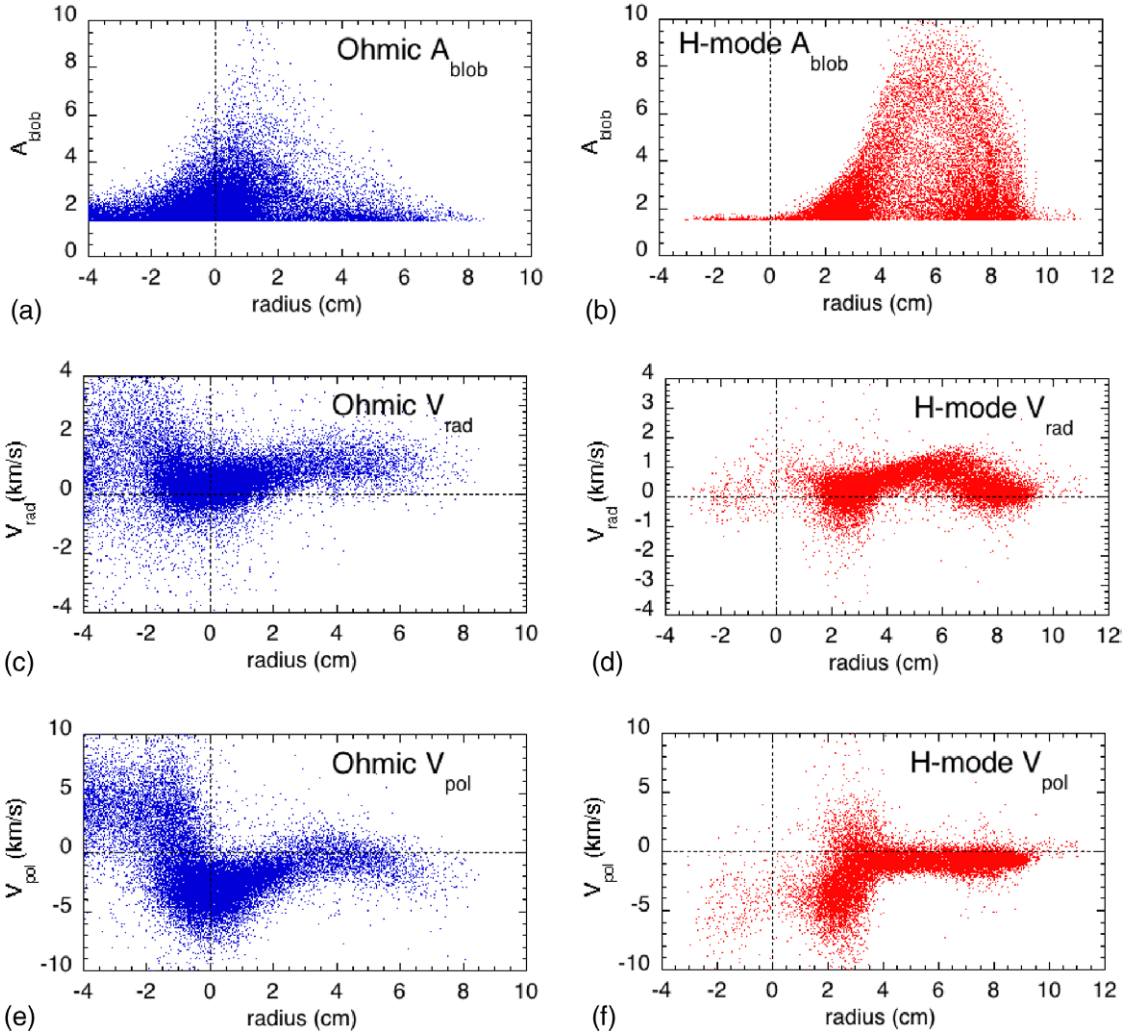

Figure 5. All blobs in the database for Ohmic (left) and H-mode (right) discharges, plotted with respect to the distance from the local separatrix; (a) and (b) show the normalized blob amplitudes, (c) and (d) show the radial blob velocities (km s^{-1}), and (e) and (f) show the poloidal blob velocities (km s^{-1}). There is a large spread in these blob properties at each radius, but also some systematic trends versus radius.

The average poloidal and radial blob velocities versus radius are shown in figures 6(c) and (d). For both Ohmic and H-mode plasmas, the magnitude of the blob V_{pol} decreases from ~3 km s^{-1} at 0 cm to ~0.5 km s^{-1} at 6 cm outside the separatrix, all in the negative direction (i.e. the ion diamagnetic and ion grad-*B* drift direction). The poloidal blob velocity at 2 cm inside the separatrix is reversed for Ohmic plasmas, as discussed previously [33]. The average blob radial velocities V_{rad} for both Ohmic and H-mode plasmas are in the range ~0.5 ± 0.5 km s^{-1} and radially outward. However, there is a large spread in V_{rad}, as shown by the error bars in figure 6(d) and individual data points in figure 5, including some inward blob velocities (see section 6).

Figures 6(e) and (f) show the average blob ellipticity (major/minor axis) and tilt angle (as defined in figure 3). The average ellipticities are similar for Ohmic and L-mode plasmas, except for larger ellipticity at 2 cm outside the separatrix for H-mode plasmas. The tilt angles are also similar between Ohmic and H-mode plasmas, averaging ~$90° \pm 10°$ in all cases, indicating poloidally elongated blob structures. Figures 6(g) and (h) show the average poloidal and radial blob size scales L_{pol} and L_{rad} (FWHM), which are in the range ~2–6 cm for all radii, with an average $L_{pol}/L_{rad} = 1.5 \pm 0.1$ for Ohmic and $L_{pol}/L_{rad} = 1.8 \pm 0.4$ for H-mode. The blob L_{pol} and L_{rad} in H-mode decrease with increasing radius, but are nearly constant versus radius in Ohmic plasmas.

In general, the average blob properties of Ohmic and H-mode plasmas in figure 6 are similar, despite the large difference in plasma parameters inside the separatrix. Comparisons of these blob properties with theoretical models are described in the following sections.

6. Radial blob velocity

The radial blob velocity is perhaps the most interesting blob parameter, since it determines the radial transport of blobs across the SOL. There has been a considerable effort to model

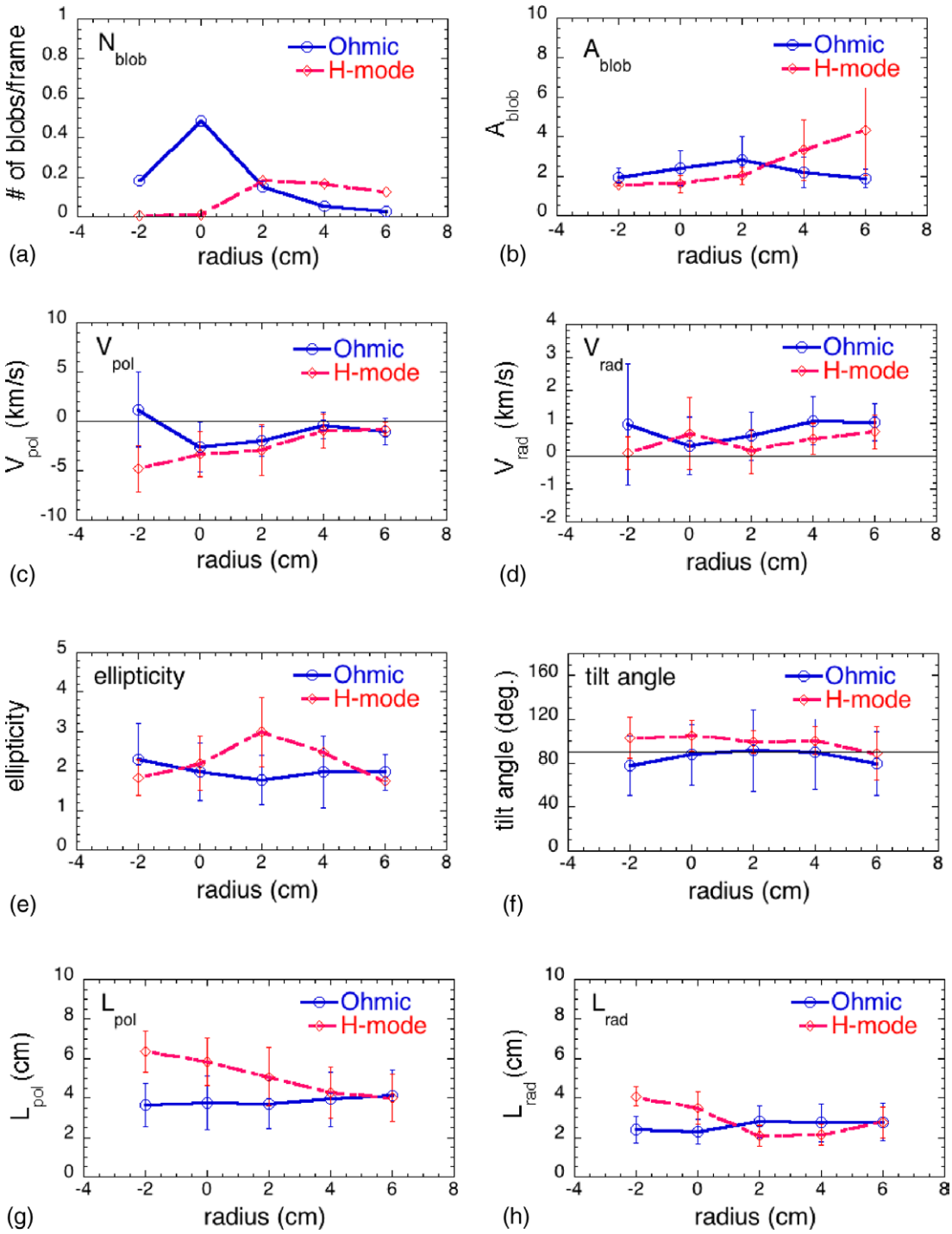

Figure 6. Average blob properties for Ohmic (blue) and H-mode (red) plasmas as a function of distance from the local separatrix; (a) shows the number of blobs per frame $N_{\rm blob}$, (b) shows the normalized blob amplitude $A_{\rm blob}$, (c) and (d) show the blob poloidal and radial velocities $V_{\rm pol}$ and $V_{\rm rad}$ in km s^{-1}, (e) and (f) show the blob ellipticity and tilt angle (in degrees), and (g) and (h) show the blob poloidal and radial scale lengths $L_{\rm pol}$ and $L_{\rm rad}$ (FWHM). Except for the blob number distribution, the average blob properties in the SOL are similar between the Ohmic and H-mode cases.

this velocity theoretically [1–3]. The radial blob velocities expected in the SC and IN regions from analytic theory relevant to these experiments are (see figure 2):

$$V_{\rm SC} = c_{\rm s}(L_{\parallel}/R)(\rho_{\rm s}/\delta_{\rm b})^2\tilde{n}/n, \qquad (3)$$

$$V_{\rm IN} = c_{\rm s}(\delta_{\rm b}/R)^{0.5}(\tilde{n}/n)^{0.5}, \qquad (4)$$

where $c_{\rm s}$ is the sound speed, $\delta_{\rm b}$ is the poloidal radius of the blob (i.e. $\delta_{\rm b} \sim L_{\rm pol}/2$), $\tilde{n}/n$ is the relative density fluctuation level in the blob, and other parameters were defined after equation (2). If the GPI light emission is linearly dependent on the local

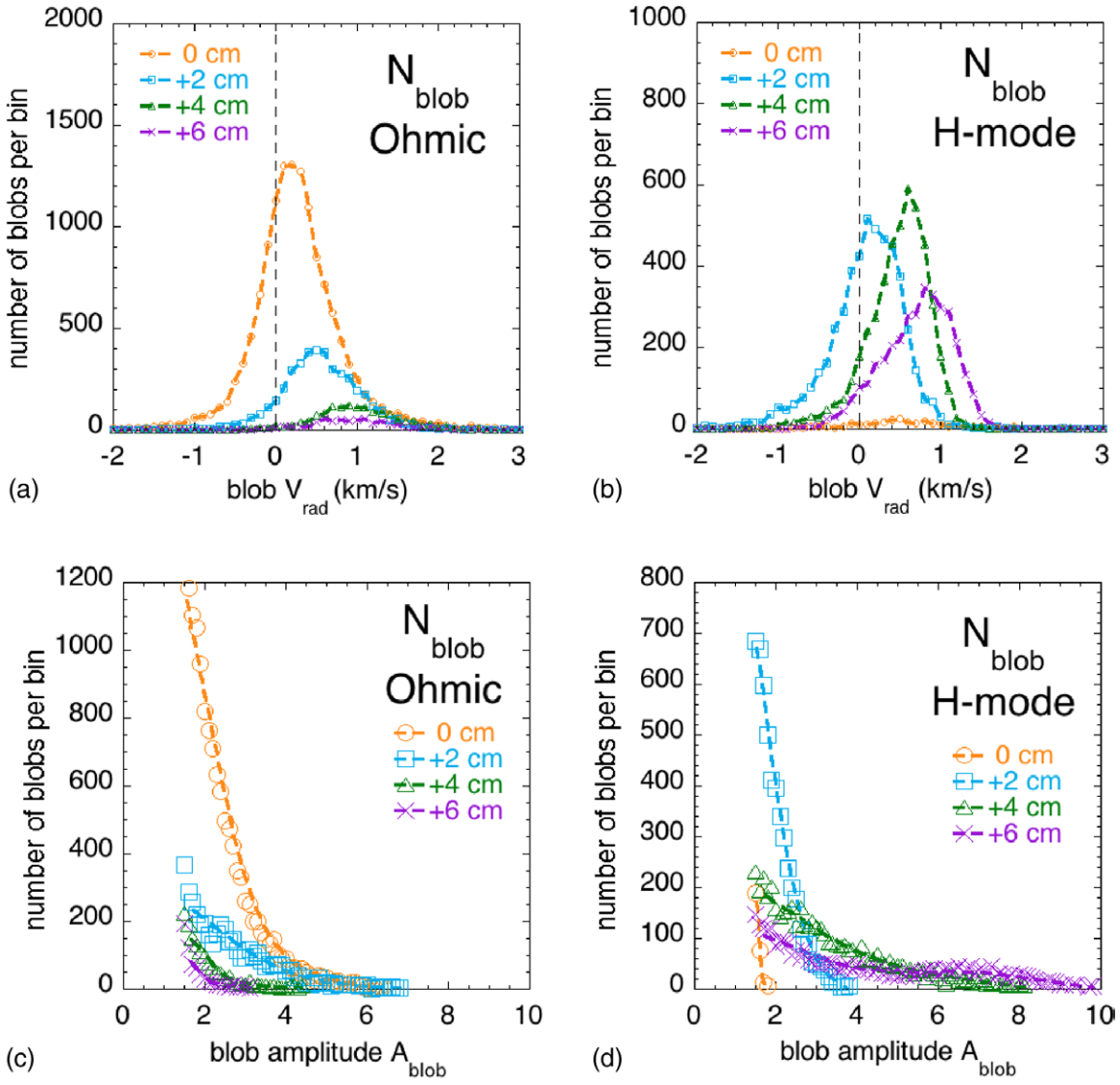

Figure 7. Distribution of the number of blobs in various radial zones as a function of the blob radial velocity in (a) Ohmic and (b) H-mode, and as a function of the blob amplitude in (c) Ohmic and (d) H-mode plasmas. The radial velocity distributions V_{rad} are always broad, with average outward (positive) velocities in all cases, but with a significant number of inward velocities, especially near the separatrix. The number of blobs is generally a strongly decreasing function of the amplitude A_{blob}.

electron density, as expected for the SOL of NSTX [33], then $\tilde{n}/n = 1-1/A_{blob}$(this is a better definition than $\tilde{n}/n = A_{blob}$ used in [33]). Thus the theoretical results for a blob propagating in a vacuum are recovered in the limit of a large A_{blob} when $\tilde{n}/n = 1$, and $\tilde{n}/n = 0$ when $A_{blob} = 1$.

Figures 7(a) and (b) show the distribution of individual radial blob velocities for the SOL region from 0 to +6 cm, binned in velocity increments of 0.1 km s^{-1}. The most probable velocities are all within 0–1 km s^{-1} in the outward (positive) direction, but these distributions are all broad with $\delta V_{rad} \sim V_{rad}$. The fraction of negative V_{rad} (inward blob velocities) generally decreases at larger radii. Figures 7(c) and (d) show the number of blobs in bins of 0.1 in amplitude for each radial zone. Above the minimum level $A_{blob} = 1.5$, the number of blobs almost always decreases strongly with the blob amplitude.

Figures 8(a) and (b) show the radial velocity of the blobs binned according to their equivalent $\tilde{n}/n = (1-1/A_{blob})$ for both for Ohmic and H-mode plasmas, with only bins having $\geqslant$5 blobs shown. Here $\tilde{n}/n = 0.33$ corresponds to the minimum level of $A_{blob} = 1.5$ and the maximum possible blob level approaches $\tilde{n}/n = 1$. The average blob V_{rad} tends to increase with increased $\tilde{n}/n$ over range $\tilde{n}/n \sim 0.33$–1.0, with a particularly clear trend for the H-mode data at +2 cm to +6 cm in the SOL. For example, at a radius of +6 cm the binned radial blob velocity in H-mode increases from $V_{rad} \sim 0.5$ km s^{-1} at $\tilde{n}/n \sim 0.4$ to $V_{rad} \sim 1.1$ at $\tilde{n}/n \sim 0.9$. Note that there were also significant statistical variations in the blob velocity in each bin, shown for example by the standard deviation error bars for selected bins for the +6 cm case in figure 8(b). These statistical variations make it difficult to see a clear trend for increasing V_{rad} with $\tilde{n}/n$ when just plotting the individual blobs without binning.

The V_{rad} data for each radial zone in figures 8(a) and (b) are fit by a power law curve with the power law exponents shown in table 2, along with R values (correlation coefficients) indicating the quality of the fit. There are strikingly good fits to the H-mode data for radii +2 cm to +6 cm, with power law

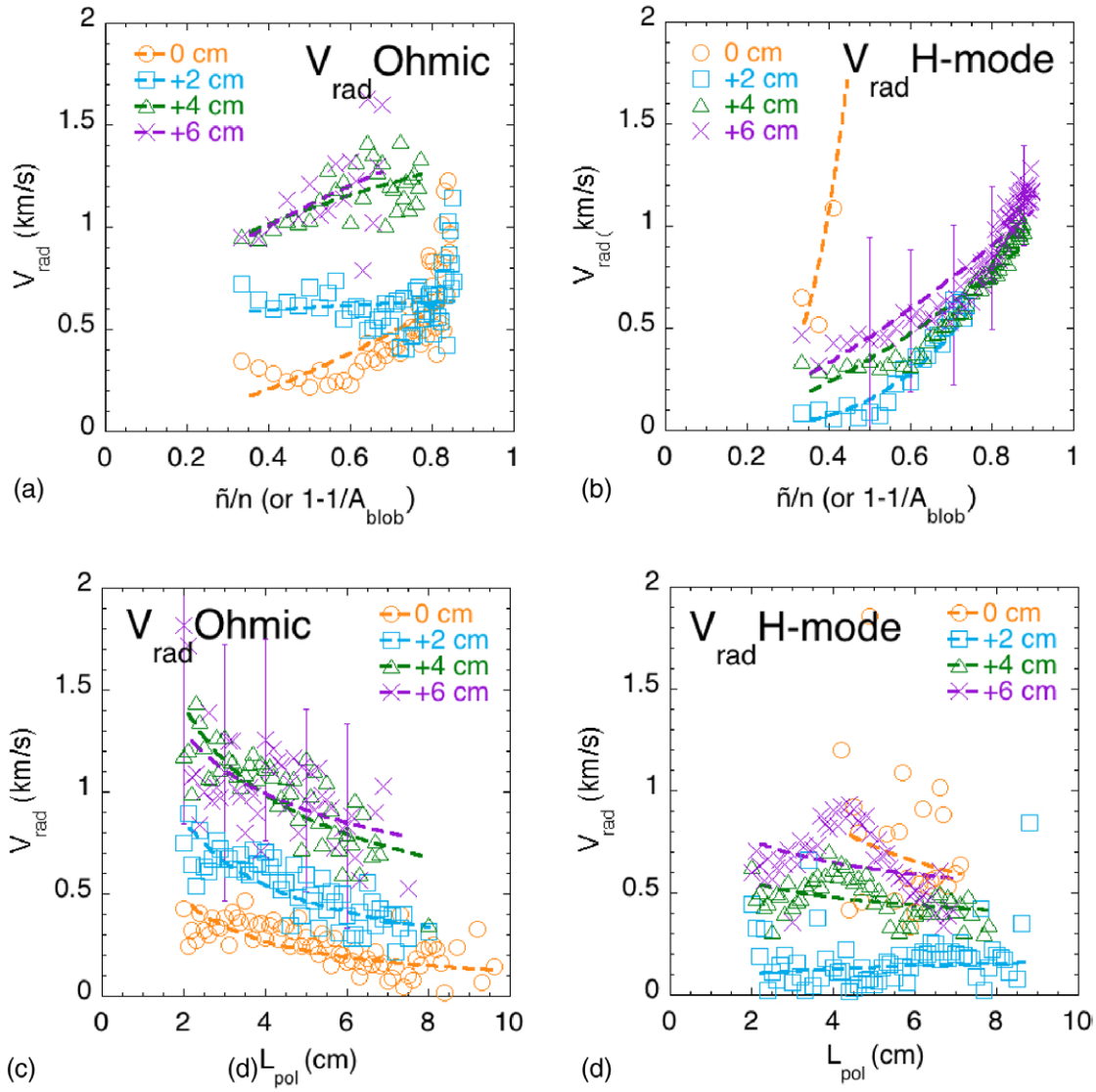

Figure 8. Blob radial velocity versus equivalent blob fluctuation level $\tilde{n}/n = 1 - 1/A_{\rm blob}$ for (a) Ohmic and (b) H-mode plasmas, binned in units of 0.1 in $\tilde{n}/n$. (b) shows a clear trend for $V_{\rm rad}$ to increase with $\tilde{n}/n$ for H-mode plasmas. The blob radial velocity versus $L_{\rm pol}$ are shown in (c) for Ohmic and (d) for H-mode, binned in units of 0.1 cm in $L_{\rm pol}$; (c) shows a clear trend for $V_{\rm rad}$ to decrease with $L_{\rm pol}$ for Ohmic plasmas. Each set of data is fit by a power law curve with exponents shown in table 2. Standard deviations of the blob distributions in selected bins are shown as error bars in (b) and (c).

Table 2. Blob radial velocity versus $\tilde{n}/n$ and $L_{\rm pol}$ power law exponents (and R values).

	$V_{\rm rad}$ versus $\tilde{n}/n$ Ohmic	$V_{\rm rad}$ versus $\tilde{n}/n$ H-mode	$V_{\rm rad}$ versus $L_{\rm pol}$ Ohmic	$V_{\rm rad}$ versus $L_{\rm pol}$ H-mode
0 cm	1.50 (0.73)	4.4 (0.92)	−0.84 (0.65)	−0.58 (0.29)
+2 cm	0.10 (0.15)	3.3 (0.97)	−0.67 (0.81)	0.29 (0.10)
+4 cm	0.32 (0.60)	1.7 (0.95)	−0.53 (0.76)	−0.20 (0.36)
+6 cm	0.44 (0.53)	1.5 (0.93)	−0.33 (0.55)	−0.22 (0.25)

exponents in the range 3.3 to 1.5 and $R \sim 0.93$–0.97. However, the Ohmic data over this radial range do not have good power law fits, with $R \leqslant 0.6$. The increasing $V_{\rm rad}$ versus $\tilde{n}/n$ shown in the H-mode data of figure 8(b) agrees at least qualitatively with the $\tilde{n}/n$ dependence of equations (3) and (4), but with larger power exponents of ~1.5–4.4 than those of in these models (i.e. 0.5 or 1.0).

Figures 8(c) and (d) shows the radial velocity of the blobs as a function of $L_{\rm pol}$ for Ohmic and H-mode plasmas, binned in increments of 0.1 cm from 2 cm to 10 cm, again using only bins containing $\geqslant$5 blobs. The average blob $V_{\rm rad}$ tends to decrease with increasing $L_{\rm pol}$ in Ohmic plasmas, but with little or no systematic variation in H-mode (three bins with slightly negative $V_{\rm rad}$ in H-mode at 0 and 2 cm are not shown). There is again a large statistical spread within each bin, shown by sample error bars in figure 8(c). These $V_{\rm rad}$ versus $L_{\rm pol}$ variations were also fit by the power law exponents shown in table 2, along with the R values. There are good power law fits ($R \geqslant 0.6$) to the Ohmic data for radii 0 cm to +4 cm, with power law exponents in the range −0.53 to −0.84. However, the H-mode data do not show any good power law fits, with $R \leqslant 0.4$. The decreasing trend of $V_{\rm rad}$ versus $L_{\rm pol}$ in the Ohmic data of figure 8(c) agrees at least qualitatively with the model of equation (3), but exponents of about −0.5 to −0.7 which are smaller

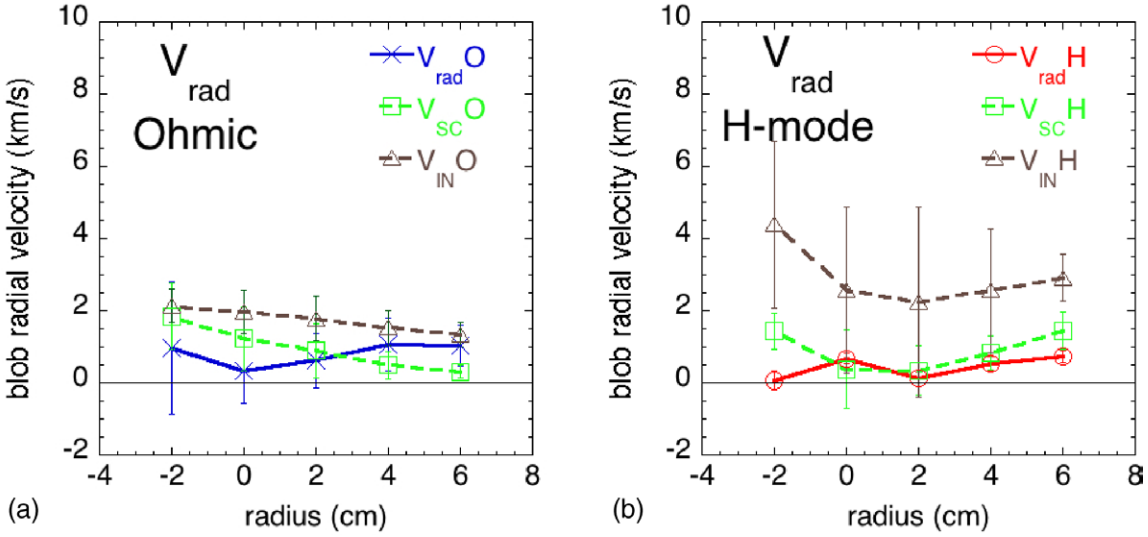

Figure 9. Comparison of average blob radial velocity versus analytic models for sheath connected (SC) and inertial (IN) for (a) Ohmic and (b) H-mode plasmas. The measured radial blob velocities are generally similar to the sheath-connected model velocities but lower than inertial velocities, although there are significant uncertainties in the model estimates, especially in the SOL.

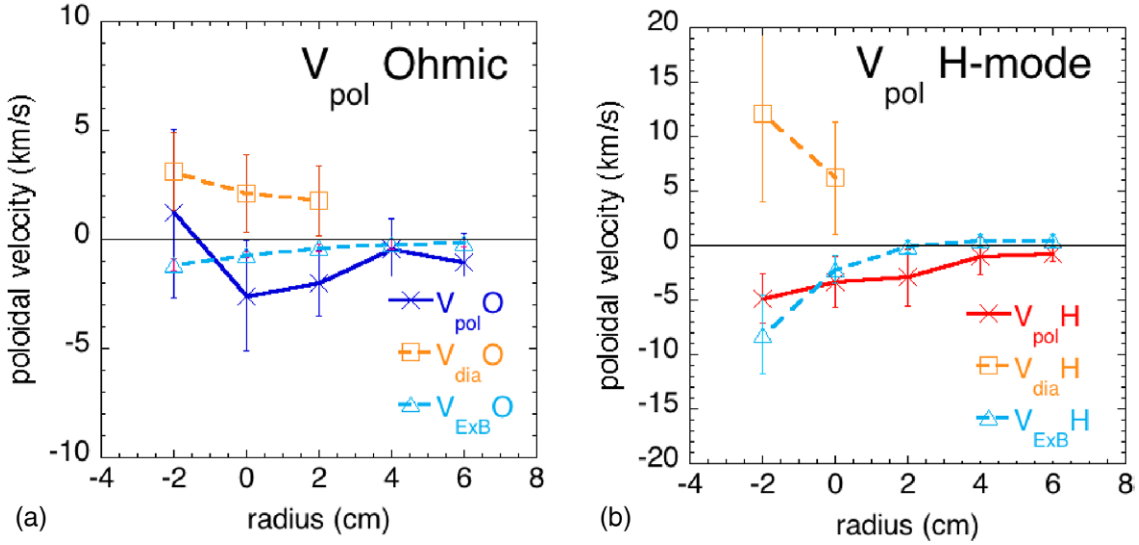

Figure 10. Comparison of the average blob poloidal velocity versus analytic models for the poloidal electron diamagnetic flow speed $V_{\rm dia}$ and the poloidal $E \times B$ flow speed $V_{E\times B}$. The measured poloidal blob velocities are in the ion diamagnetic direction in the SOL and close to those expected from the $V_{E\times B}$ due to the sheath potential (estimated from the $T_{\rm e}$ gradient).

than that model (i.e. -2). However, the trends in these data disagree with the model of equation (4), which has a $+0.5$ power law exponent.

An attempt was made using multiple linear regression analyses to fit all of the whole data set of individual $V_{\rm rad}$ blob speeds jointly with $\tilde{n}/n$ and $L_{\rm pol}$ for each radial zone, without the binning as done for figure 8. However, no good power law fits were found from any of those regression analyses, i.e. the random variations in the blob data overwhelmed any simple power-law relationship. There was no significant linear cross-correlation between $\tilde{n}/n$ and $L_{\rm pol}$ in any of these cases ($R \sim$ 0.1–0.4), so the trends for $V_{\rm rad}$ versus $\tilde{n}/n$ and $L_{\rm pol}$ in figure 8 appear to be independent of each other.

It is interesting that the H-mode data of figure 8(d), particularly at $+4$ and $+6$ cm, suggests at first an increasing trend with $L_{\rm pol}$, and then a decreasing trend. This is qualitatively similar to the blob regime model of figure 2 when the transition from inertial (small blob, $\delta_{\rm b} < \delta_{\rm b*}$) to sheath-connected (large blob, $\delta_{\rm b} > \delta_{\rm b*}$) regimes takes place. The observed breakpoint at $L_{\rm pol} \sim 4$ to 5 cm is similar to the expected transition value of $L_{\rm pol} \sim 2\delta_{\rm b*} \sim 3$ to 4 cm for these data. A similar regime transition of blob velocity with poloidal size scale has been previous observed in Torpex [23]. Note that the additional dependences of $V_{\rm rad}$ on $c_{\rm s}$ and $\rho_{\rm s}$ (i.e. the $T_{\rm e}$ in the blob) should also be taken into account in comparisons of $V_{\rm rad}$ with theory, but these measurements were not available for individual blobs.

Figure 9 shows a comparison of the radial profile of the measured blob velocities $V_{\rm rad}$ with radial profiles of the calculated $V_{\rm SC}$ and $V_{\rm IN}$ for Ohmic and H-mode plasmas in this

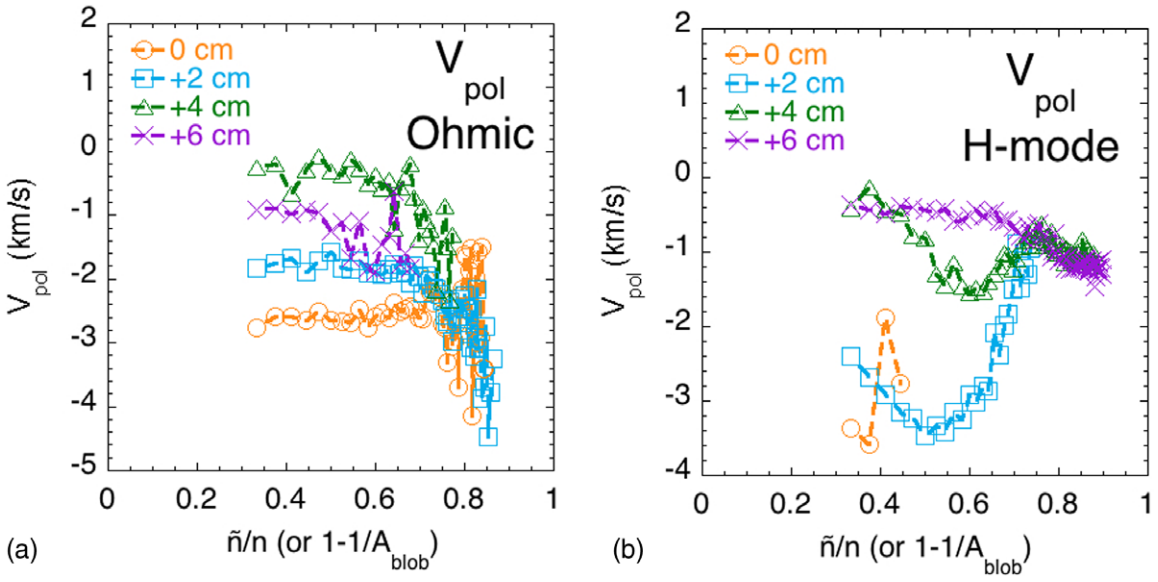

Figure 11. Blob poloidal velocity V_{pol} versus blob fluctuation level $\tilde{n}/n = 1-1/A_{blob}$ for (a) Ohmic and (b) H-mode plasmas, binned in units of 0.1 in $\tilde{n}/n$. There is a trend for V_{pol} to become increasingly negative for high $\tilde{n}/n$ in Ohmic plasmas for radii from +2 to +6 cm, and for V_{pol} for H-mode plasmas to peak in the negative direction near $\tilde{n}/n \sim 0.5$–0.6.

database. Here all blobs with amplitude $A_{blob} \geqslant 1.5$ are averaged together for each radial zone (with their standard deviation shown as an error bar). The averaging over all blobs for figure 9 does not reflect the systematic variations in blob radial velocity described in figures 7 and 8; however, those variations are relatively small (± 0.5 km s^{-1}) in the broader context of figure 9, which aims to give a rough comparison of experimental versus theoretical blob trends. The evaluations of the theoretical V_{rad} use the average electron temperatures versus radius from figure 1 to compute c_s, and the average $L_{pol}/2$ versus radius to compute δ_b (see section 8), and $\tilde{n}/n$ is taken to be the average of $(1 - 1/A_{blob})$ for each zone, with $R = 150$ cm and $L_{\|} = 500$ cm are assumed for all cases.

The measured V_{rad} for blobs in Ohmic plasmas is within ~0.5–1.0 km s^{-1}, which is roughly consistent (within the joint error bars) with the V_{SC} and V_{IN} in figure 9(a), which are in the range ~0.2–2 km s^{-1}. The measured V_{rad} for blobs in H-mode plasmas is within ~0–1 km s^{-1}, which is close to V_{SC} in figure 8(b), but x5-10 smaller than the estimated V_{IN}. Thus the measured V_{rad} in the SOL are fairly well described by sheath-connected model velocities in both cases. For the far SOL this is as expected from the blob regime diagram in figure 2. It is not clear why the SC scaling should apply to the H-mode data near or inside the separatrix (for the Ohmic case, the IN and SC estimates are not very different.) The error bars in the theoretical velocities based on uncertainties in c_s, A_{blob}, and L_{pol} are large, especially outside +2 cm where the data are very uncertain, so this comparison is limited.

7. Poloidal blob velocity

The poloidal velocity of edge turbulence is usually considered to be dominated by the local diamagnetic and/or $E \times B$ poloidal flows. However, in the SOL where the fluctuation levels are large, these fluid flows will also be fluctuating in space and time, and blob tilting in theory can also cause blob poloidal motion [31].

Figure 10 shows a comparison of the average poloidal blob velocities V_{pol} versus radius with the estimated electron diamagnetic and $E \times B$ flow velocity for Ohmic and H-mode plasmas in this database. The diamagnetic velocity was taken to be $V_{dia} = c_s\rho_s/L_n$ in the electron direction, and the $E \times B$ velocity was estimated by assuming a local SOL potential of ~$3T_e$, as expected from connection to the divertor plate sheath (both using B_t in the GPI region). Particularly for the H-modes inside the separatrix, the actual electric field (which was not measured in these discharges) may differ from this estimate. The error bars on the blob velocities are the standard deviations from the blob database, and the error bars for V_{dia} and $V_{E\times B}$ were estimated from uncertainties in the Thomson measurements (figure 1).

The poloidal $E \times B$ velocities in the SOL of ~1–3 km s^{-1} in figure 10 are in the same range and direction as the measured poloidal blob velocities for both Ohmic and H-mode cases, at least to within the joint uncertainties. The electron diamagnetic velocities are of the opposite sign, and have considerable uncertainty due to the difficulty in estimating L_n from the Thomson data. In Ohmic plasmas, reversal of the measured blob V_{pol} from the electron diamagnetic direction inside the separatrix to the $E \times B$ (i.e. ion direction) in the SOL is commonly seen in other experiments and simulations [31]. When T_i effects are important, as they likely are for the H-mode case here, the ion diamagnetic velocity is also relevant. Ongoing simulation studies [10] are exploring the relationship of the blob velocity to the diamagnetic and $E \times B$ velocities.

The variation of poloidal blob speeds versus $\tilde{n}/n = (1-1/A_{blob})$ is shown in figure 11, binned and plotted similarly to the radial speeds in figure 8 and fit with smooth curves (not power laws). For Ohmic plasmas in figure 11(a), the blob V_{pol} appears to become increasingly negative

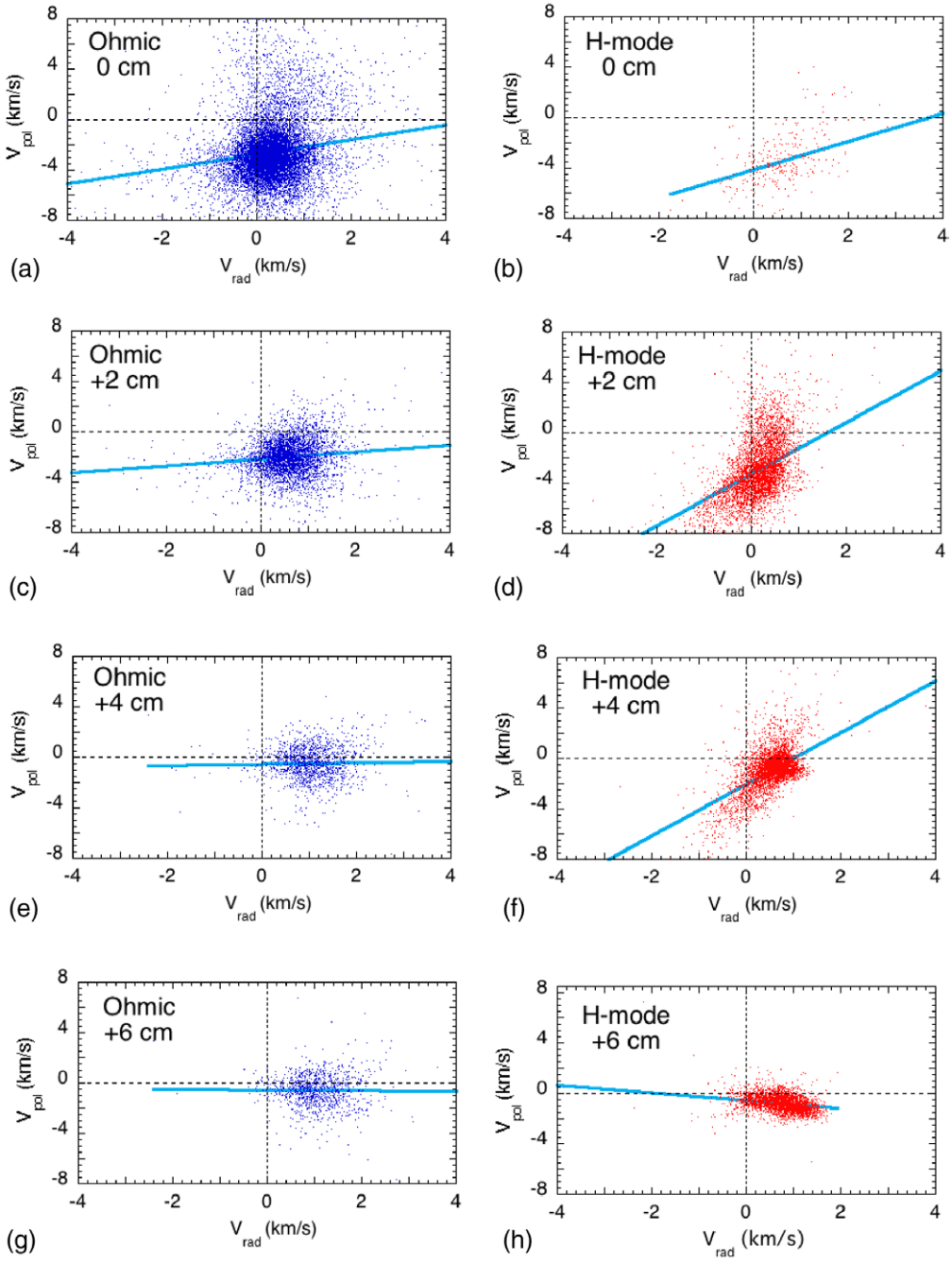

Figure 12. Poloidal blob velocity V_{pol} versus radial blob velocity V_{rad} for radial zones in the SOL, with Ohmic plasmas at the left and H-mode plasmas at the right, along with linear fit lines in blue. There is little correlation of V_{pol} and V_{rad} for the Ohmic cases, as shown by the R values in table 3, but there is a moderate correlation of V_{pol} and V_{rad} for the H-mode cases at 0 cm to +4 cm.

(in the ion diamagnetic direction) with increasing $\tilde{n}/n$ for radii between +2 to +6 cm, although it is nearly constant versus $\tilde{n}/n$ at 0 cm. This is similar to the behavior of V_{rad} in figure 8(a), with the magnitude of both V_{rad} and V_{pol} increasing with $\tilde{n}/n$, and suggests a coupling between V_{rad} and V_{pol} at large $\tilde{n}/n$, which is expected in a general sense from the Reynolds stress mechanism [31], i.e. fluctuation driven flows. However, this particularly clear experimental demonstration has not (to our knowledge) been previously reported for poloidal blob motion, and is not yet understood in detail (see discussion later in this section). The poloidal velocity in H-mode plasmas at radii of +2 cm and +4 cm in figure 11(b) has a maximum in the ion diamagnetic direction for $\tilde{n}/n$ ~ 0.5–0.6, which is not expected or understood, as discussed in section 10.2.

The empirical relationship between V_{pol} and V_{rad} for all blobs in the SOL for Ohmic and H-mode plasmas is shown in figure 12, along with linear fits to the data in each case. The linear correlation coefficient R between these two quantities is small for the Ohmic cases ($\leqslant$0.25), as shown in table 3. However, there is fairly high correlation (~0.54) between these two velocities for the H-mode cases between +2 cm and +4 cm, with V_{pol} becoming closer to zero or more positive

Table 3. Linear fit coefficients of V_{pol} versus V_{rad} (R values in parentheses).

	Ohmic	H-mode
0 cm	0.60 (0.21)	1.1 (0.53)
+2 cm	0.28 (0.13)	2.1 (0.52)
+4 cm	0.06 (0.03)	2.1 (0.56)
+6 cm	−0.030 (0.02)	−0.31 (0.25)

(in the electron drift direction) at higher V_{rad}. Surprisingly, at +6 cm V_{pol} becomes more *negative* for larger V_{rad}, although the correlation coefficient is relatively low (0.25).

One possible mechanism for a correlation between V_{pol} and V_{rad} is the tilt angle of the blob charge dipole, which would tend to convert what would have been radial motion into poloidal motion. This effect would be zero for tilts of +90°, for which the major axis of the elliptical blob is in the V_{pol} direction, which is where most of the blob tilts lie (see figure 6(f) and the next section). A test of this mechanism was done by re-plotting the data in figure 11 as V_{pol} versus $V_{rad} \times \cos(\text{tilt})$, which would show a positive correlation if this mechanism was dominant. However, the cross-correlation coefficients between these two variables were $R \leqslant 0.4$ for all cases, implying that this was not a strong effect in this data. Further constraining the data to $A_{blob} > 3$ did not significantly improve these cross-correlations.

8. Blob structure

The average blob sizes in the poloidal and radial (i.e. vertical and horizontal) directions are plotted in figures 6(g) and (h). These size scales were nearly constant within the radial range from 2 cm inside to 6 cm outside the separatrix, with $L_{pol} = 3.6 \pm 1.3$ cm for Ohmic and $L_{pol} = 4.5 \pm 1.3$ cm for H-mode, and $L_{rad} = 2.5 \pm 0.8$ cm for Ohmic and $L_{rad} = 2.4 \pm 0.8$ cm for H-mode. However, there was a nearly factor-of-two increase in L_{pol} for the innermost radii of −2 cm, perhaps due to the increase in the drift wave parameter ρ_s at higher T_e. There was no significant trend for the blob sizes to increase with the blob amplitudes at any radius, in part due to the definition of blob size as the FWHM of the blob ellipse fit (i.e. not the size at some fixed normalized level).

There is no simple theoretical prediction for the blob size scales, since the blob birth processes are not well understood. However, the turbulence correlation scale lengths at −2 cm over a wide database in NSTX [33] were roughly consistent with $k_{pol}\rho_s \sim 0.1$ (using the edge B_t), and the blob size data at −2 cm was consistent with that scaling.

Plots of the blob tilt angle versus ellipticity for Ohmic and H-mode plasmas for various radial zones are shown in figure 13, along with linear fits to the data points. Here the ellipticity is defined as the ratio of major to minor radii of the elliptical fits to the blobs, and the tilt angle is the clockwise angle of the major axis with respect to the radial direction toward the plasma center. The average tilt angles over the range 0–6 cm in the SOL are 89° ± 33° for Ohmic and 100° ± 14° for H-mode plasmas, corresponding to blobs nearly elongated in the poloidal direction (90°). These tilts are qualitatively what would be expected from the shear in the V_{pol} indicated in figures 11 and 6(f): both less than and greater than 90° in the Ohmic case (i.e. with tilts looking like '\' inside the separatrix and '/' in the near SOL, respectively), and greater than 90° in the H-mode case ('/'). There are no strong variations of tilt with ellipticity, except for a larger spread in tilt for low ellipticities, which is most likely due to uncertainties in the fitting for small ellipticities. There are also no strong variations of tilt or ellipticity with normalized blob amplitude in this database.

The relationship of the blob shape and tilt to the edge sheared flows in NSTX was previously discussed in [31]. Since there were no direct measurements in NSTX of the edge Reynolds stress from the fluctuating local fluid velocities $R = \langle \delta V_{pol} \delta V_{rad} \rangle$ (e.g. from probes or spectroscopy), a 'Reynolds stress proxy' (RSP) was developed in the paper cited above to estimate the local Reynolds stress based on the blob structure itself:

$$\text{RSP} = -(\sin 2 \times \text{tilt})(1 - \text{ellipticity}^2), \tag{5}$$

where the tilt angle and ellipticity are defined as above.

Figure 14 shows the radial profile of RSP for all blobs for (a) Ohmic and (b) H-mode plasmas and with smoothed fits to this data (magenta lines), along with the average V_{pol} profiles. First, it is significant that nearly the full range of RSP values (−1 to 1) is attained, particularly for the Ohmic case. This indicates that significant shearing stresses are acting on the blobs. The large spread in instantaneous RSP values at a particular radius is suggestive of fluctuating zonal flows. Theoretically, the dimensionless shearing parameter $V'_{pol}\tau$ provides a simple estimate of when local $E \times B$ shear significantly affects blob tilt and ellipticity [31]. Here V'_{pol} is the background shearing rate and $\tau \sim L_{rad}/V_{rad}$. For the Ohmic data presented in figure 14(a) we estimate a maximum shearing rate just inside the separatrix of $V'_{pol} \sim 1.5 \times 10^5$ s^{-1} and $\tau \sim 10^{-5}$ s resulting in $V'_{pol}\tau > 1$ consistent with significant shearing effects. From radial force balance, Reynolds stress drives poloidal flows and we expect that flow should be driven in the direction of $-\partial_x(\text{RSP})$. This is consistent with the negative dip in V_{pol} in figure 14(a) between the radii −3 and 0 cm where the RSP variation is most pronounced. Qualitatively, these RSP-related observations are similar to those reported on in [31] for another NSTX Ohmic discharge. They suggest that in the Ohmic case sheared flows both affect and are affected by the blobs.

The present dataset also allows a similar analysis of an H-mode case, which was not attempted in [31]. Figure 14(b) shows slightly less total variation in the RSP. We estimate a maximum shearing rate at +2 cm of $V'_{pol} \sim 1.2 \times 10^5$ s^{-1} and $\tau \sim 4 \times 10^{-5}$ s again resulting in $V'_{pol}\tau > 1$, with the implication of significant shearing effects on the blobs at this location. The most significant spatial gradient of the RSP is in the range +3 to +7 cm. The sign of the gradient implies that Reynold's flows should be driven in the positive V_{pol} direction, but this is not observed. Similarly, there is no positive correlation between the RSP gradient and the flow in the range

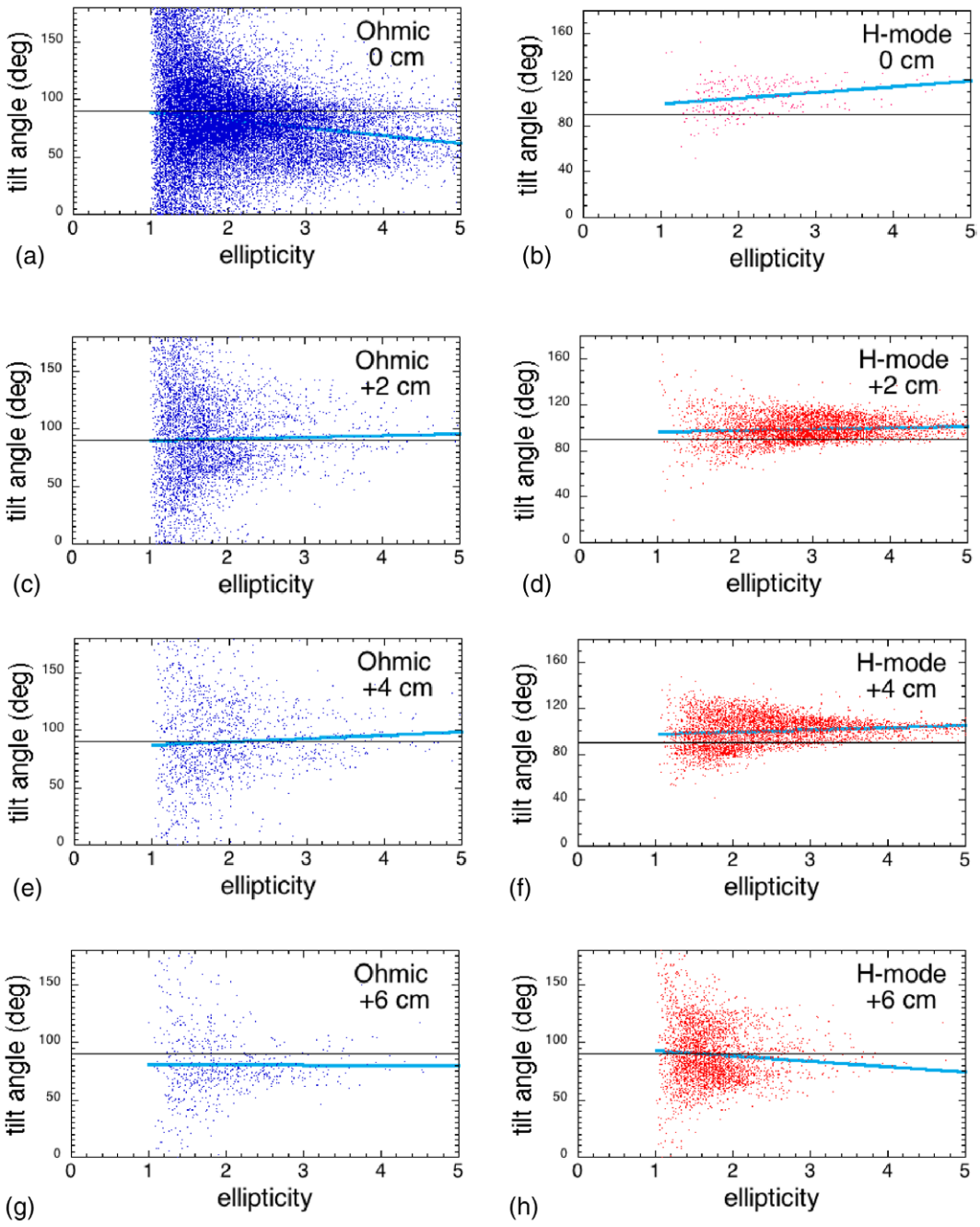

Figure 13. Plots of the blob tilt angle versus ellipticity for Ohmic (left) and H-mode (right) for various radial zones in the SOL, along with linear fits in blue (tilt is defined in figure 3). The average tilt angles are near 90° (black lines), corresponding to blobs elongated in the poloidal direction. There is little or no systematic variation of tilt with ellipticity.

7 to 10 cm. This suggests that some mechanism other than Reynolds stress dominates flow drive. Inside the separatrix, there may be too few H-mode blobs to make reliable statements. Theoretically, Reynolds driven flows might be expected to be subdominant relative to mean pressure-gradient driven $E \times B$ flows, and in the SOL to sheath driven $E \times B$ flows [10, 31]. In summary the Ohmic RSP data suggests that blobs and flows mutually affect each other, while the H-mode data suggests that flows affect the tilting of the blobs, but the blobs do not dominate the creation of the flows.

9. Blob SOL width

One potential result of blob structure and motion is a broadening of the scrape-off layer (SOL) width of particles and heat due to outward blob motion across the separatrix. Recently there have been many experimental (e.g. [35, 36]) and theoretical (e.g. [37, 38]) studies of the SOL width of tokamaks, motivated mainly by the high divertor plate heat flux expected in ITER. At present it is not clear what mechanisms determine the SOL width in present devices.

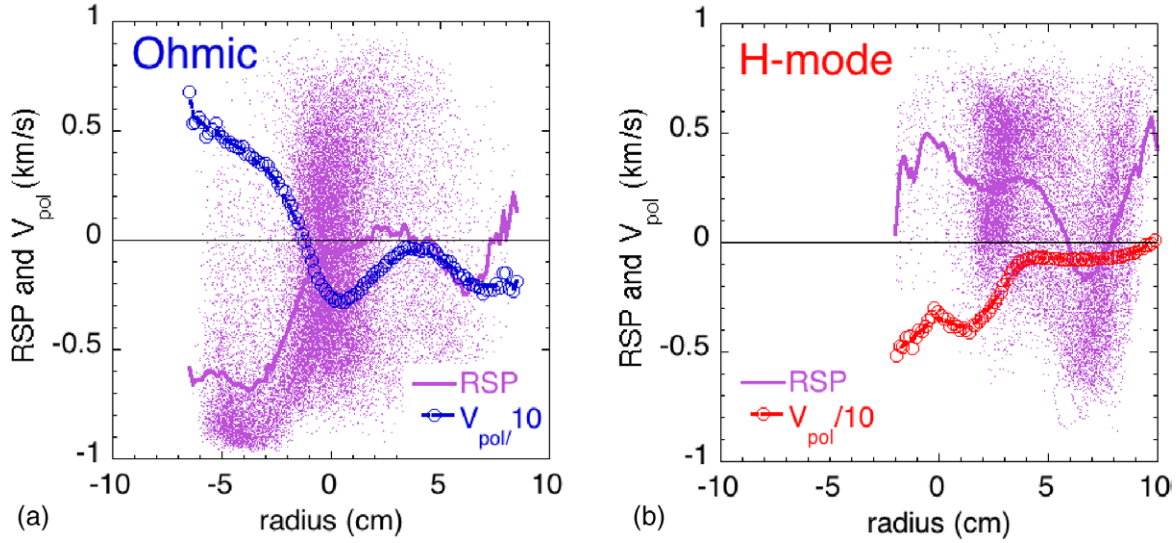

Figure 14. Radial profiles of the Reynolds stress proxy (RSP) for all (a) Ohmic and (b) H-mode plasmas, along with smoothed fits to the RSP data (purple lines) and the average blob V_{pol} profiles (in units of km s^{-1}/10). The Ohmic RSP data suggest that blobs and flows mutually affect each other, while the H-mode data suggest that flows affect the tilting of the blobs, but the blobs do not dominate the creation of the flows.

The simplest model for the *blob contribution* to the density SOL width assumes that blobs move radially outward at a speed V_{rad} across the separatrix, and that they carry with them all the ions within the blob. If this assumption is true, then the radial distance over which these blob ions move into the SOL is therefore:

$$\lambda_n \sim V_{rad}\tau_{blob}, \quad (6)$$

where τ_{blob} is the lifetime of the blobs in the SOL. However, at the same time that the blobs are moving radially in the SOL, the blob ions are also moving along the B field line to the divertor plates, where they are eventually absorbed (or recycled). For the present database, the average lifetime of blobs in the GPI field of view is $\tau_{blob} \sim 23$ μs for the Ohmic cases and $\tau_{blob} \sim 36$ μs for the H-mode cases, most of which is spent in the SOL. This is significantly less than the timescale for parallel ion motion along B of $\tau_{sol} \sim 2L_{\|}/c_s \sim 500$ μs, assuming an ion speed of $V_{i,\|} \sim c_s/2 \sim 10^6$ cm s^{-1} and a parallel connection length $L_{\|} \sim 500$ cm. Thus τ_{blob} is used in equation (6) instead of τ_{sol}.

For a typical blob radial velocity of $V_{rad} \sim 0.5$ km s^{-1} in the SOL (see figure 6(d)) and a typical blob lifetime of $\tau_{blob} \sim 30$ μs, the resulting estimate of the blob-induced density SOL width from equation (5) is $\lambda_n \sim 1.5$ cm. This is within a factor-of-two of the density decay scale length measured by Thomson scattering just outside the separatrix in these experiments as shown in figure 1(f); namely, $\lambda_n \sim 3$ cm for the Ohmic case and the $\lambda_n \sim 1$ cm for the H-mode case. This level of agreement is as good as can be expected, considering the many factors not taken into account in this simple analysis; for example, the ionization and recycling source in the SOL, the ion neoclassical orbit effects and flows, and turbulent (non-blobby) particle diffusion into the SOL.

The simplest model for the effect of blobs on the SOL electron temperature width assumes electrons are transported radially at V_{rad} along with the blob density, and that their heat content diffuses along B to the divertor plate due to the competition between electron thermal motion and collisions. The resulting electron temperature SOL width due to blobs is:

$$\lambda_{T_e} \sim V_{rad}\tau_{II,e}. \quad (7)$$

The parallel electron heat conduction time $\tau_{II,e} = 3/2L_{II}^2/\chi_{II,e}$ [35] depends on the electron thermal conductivity $\chi_{II,e}$, and for the separatrix conditions here is roughly $\tau_{II,e} \sim 20$ μs. Since this time is (marginally) less than τ_{blob}, the blob lifetime is not dominant in determining λ_{T_e} as it was for λ_n. Assuming $V_{rad} \sim 0.5$ km s^{-1}, the blob-induced electron temperature SOL width is thus $\lambda_{T_e} \sim 1$ cm, which is $\times$2–3 lower than the measured T_e scale lengths of $\lambda_{T_e} \sim 2$–3 cm at the separatrix as shown in figure 1(c). There are again several reasons why equation (7) should not be an accurate estimate of the temperature SOL width; for example, the collisional electron heat transport along B may be affected by heat flux limits due to kinetic effects [35], there may be significant electron energy loss due to radiation in the SOL, and some of the radial electron heat flux may be due to broadband turbulence rather than blobs.

Note that the SOL width estimates of equations (6) and (7) apply only to the *blob-like* components of the radial particle and heat flux, and do not imply that *all* radial fluxes in the SOL are due to blobs. More direct measurements of blob transport have been made using Langmuir probes to directly measure the density and temperature of the blobs [32, 39–41], with the general result that blobs appear to contribute significantly to particle and heat transport in the SOL of tokamaks. However, some assumptions are still needed for these estimates, e.g. about the poloidal distribution of the blob-induced transport.

Estimates of the heat flux width, λ_q were made for the H-mode cases from measurements of the divertor heat flux via infrared thermography [42] using a fast (1.6 kHz) IR camera [43]. The radial heat flux profiles in these discharges are highly structured, resulting in a profile that is poorly described by the semi-empirical diffusive-Gaussian model [36]. Because of

this, the FWHM of the near-SOL heat flux profile is used to estimate the heat flux width by averaging 20 frames (12.5 ms) of thermography data about the time of interest. The divertor heat flux width $\lambda_{q,\,FWHM}^{div}$ is found to range from 88–116 mm in these discharges. When magnetically mapped to the outer midplane, the magnetic flux expansion, f_x, is $11.3 \leqslant f_x \leqslant 12.6$ as calculated from EFIT02 reconstructions and averaged spatially 5 mm radially outward from the outer strike point and temporally over the same 12.5 ms as the heat flux profiles. This leads to an inferred midplane heat flux width of $\lambda_{q,\,FWHM}^{mid} = 7.2 - 10.2$ mm, which is in reasonable agreement with other upstream quantities and with the SOL heat flux widths inferred for blobs above.

10. Summary and discussion

Section 10.1 summarizes the results of this paper, section 10.2 discusses some open physics issues concerning the 2D blob velocity, section 10.3 discusses the definition of a blob, section 10.4 describes comparisons with previous experiments, and section 10.5 suggests directions for further experiments.

10.1. Summary

This paper described the 2D radial versus poloidal blob structure and motion in the edge and SOL of NSTX for representative Ohmic and H-mode discharges, as measured using a gas puff imaging (GPI) diagnostic. A large database was made for these two types of shots with individual blob amplitudes, spatial sizes, shapes, and velocities as a function of radius, which was used for both empirical correlations and comparisons with blob theory. This extends a previous paper on GPI results in NSTX in which only the average blob properties for each shot were described [33].

In general, there was little difference between the blob properties in the SOL for Ohmic and H-mode discharges, as illustrated in figure 6. Typical average blob velocities in the SOL were $V_{pol} \sim 2 \pm 1$ km in the ion diamagnetic drift direction and $V_{rad} \sim 0.5 \pm 0.5$ km s^{-1} in the outward direction, with spatial scales $L_{pol} \sim 4 \pm 1$ cm and $L_{rad} \sim 2.5 \pm 1$ cm. Elliptical fits to the blob structure in the radial range 0 cm to +6 cm in this database had an ellipticity of $\sim 1.6 \pm 0.6$ for the Ohmic case and 1.9 ± 0.6 for the H-mode case, which is consistent with the results from blob analysis of a larger set of NSTX shots [33], in which the analysis was done in exactly the same way. The tilt angles $\sim 90° \pm 10°$, i.e. with the long axis nearly in the poloidal direction. The clearest difference between Ohmic and H-mode cases was found in the number of blobs detected near or just inside the separatrix, which was much lower in H-mode plasmas than Ohmic plasmas. As usual for blob studies in tokamaks, there was a fairly wide scatter in the individual blob properties even for a given shot and radial zone, as illustrated in figures 5–7.

There was a clear trend for the blob V_{rad} in H-mode plasmas to increase with blob amplitude (i.e. $\tilde{n}/n$) in the binned data of figure 8(b), and for V_{rad} to decrease with the blob poloidal size scale L_{pol} in Ohmic plasmas in the binned data in figure 8(c). These trends were less clear in the un-binned database due to the large scatter in V_{rad}. The power law fits to the trends in the binned data versus $\tilde{n}/n$ (table 2) were qualitatively consistent with analytic blob theory (equations (3) and (4)), but with larger power law exponents. The radial profile of V_{rad} agreed fairly well with the sheath-connected blob model to within the joint uncertainties, as shown in figure 9. The blob poloidal velocities were roughly consistent with the expected $E \times B$ drift motion in the SOL, as shown in figure 10, although there were also some systematic variations of V_{pol} with the blob $\tilde{n}/n$, as shown in figure 11.

The empirical relationships between the blob V_{pol} and V_{rad} at various radii did not show strong correlations between these two speeds, as shown in figure 12 and table 3. There was also little or no empirical correlation between the blob tilts and their ellipticity, as illustrated in figure 13. Finally, a theoretical model for the Reynolds stress-induced poloidal blob velocity was tested using a Reynolds stress proxy [31], which suggested that sheared flows both affect and are affected by the blobs, at least for the Ohmic cases, as shown in figure 14.

10.2. Physics of 2D motion of blobs

Perhaps the most interesting new result in this paper was the systematic increase in the blob radial velocity with increased blob amplitude for the H-mode cases shown in figure 8(b). Although such an increase is a robust prediction of blob models such as equations (3) and (4), due to an increase in the blob poloidal electric field with increased blob amplitude, to our knowledge this result was not found in any previous tokomak experiments. Also interesting was the decrease in blob radial velocity with blob poloidal size in Ohmic plasmas as shown in figure 8(c), which is also qualitatively consistent with the decrease in local poloidal electric field with blob size in the sheath-connected model of Equation (3). Figure 8(d) hints at a non-monotonic dependence of the radial blob velocity on blob poloidal size in H-mode plasmas, which may be suggestive of inertial effects for smaller size blobs.

The poloidal motion of blobs is less clearly defined in the analytic blob theory. Small amplitude blobs should 'go with the flow' in the poloidal direction, but in [31] it was shown that in the Ohmic case the Reynolds stress arising from SOL currents and radial inhomogeneity is of sufficient strength and direction to explain the V_{pol} reversal of blob tracks across the separatrix. If this nonlinear Reynolds mechanism is correct, then it would be expected to drive V_{pol} increasingly negative as A_{blob} increases, apparently consistent with the increase in the (negative) Ohmic V_{pol} at large $A_{blob} > 4$ ($\tilde{n}/n > 0.75$) in figure 11(a). On the other hand, figure 11(b) shows that for the H-mode cases with $A_{blob} > 4$, $V_{pol} \sim -1$ km s^{-1} at all radii. Several mechanisms particular to large amplitude blobs can result in motion in the observed ion diamagnetic direction, such as positive charging and rotation [31, 44] or finite ion pressure [8, 10, 14, 45]. However, at present it is not understood why any of these mechanisms would result in a nearly constant V_{pol} for all SOL radii when A_{blob} exceeds a threshold.

10.3. Definition of a blob

The theoretical concept of an isolated blob in the SOL is well defined and allows straightforward analytic modeling of blob motion [1–3]. However, the blobs observed in tokamak experiments are never completely isolated, so there is no universal definition of a blob in the experimental literature. The blobs in the present paper were defined by a 2D blob tracking algorithm appropriate for the GPI diagnostic (section 4), but blobs in 0D or 1D measurements are defined differently, e.g. using a 2.5 × rms-level threshold [46], or characterized by a threshold for the skewness or kurtosis of a single-point time series. Thus it is difficult to compare results on blobs across different experiments, for example with respect to the blob creation process, the blob number density, and blob transport effects.

This lack of clear definition for a blob is not surprising in the context of neutral fluid turbulence, where the analogous concept of a 'coherent structure' is also not well defined despite many years of research [47, 48]. Coherent structures can sometimes be seen clearly in fluids, e.g. as tornados in thunderstorms, or 'bubble and spike' structures in nonlinear Rayleigh–Taylor instabilities, but usually they are hidden within the complexity of the turbulence. Although the initial search for 'blobs' in a tokamak edge [49] was motivated by coherent structures in fluids, those results were *negative*, in that no clear evidence for 'coherent structure' in plasma blobs was found. In the present paper the strongest evidence for blobs as coherent structures is the degree to which the results in figures 8(b), (c) and 9 agreed at least qualitatively with the analytic blob theory.

Further attempts to understand the role of blobs in the tokamak edge could directly compare specific blob measurements with synthetic diagnostics from computational simulations. In that case a unique definition of a blob is not crucial, since multiple aspects of the blob structure and motion can be compared. Clarification of the physics of blobs can be pursued by a detailed comparison of the computational results with the simplified analytic models.

10.4. Comparisons with other tokamak measurements

The properties of blobs in the SOL of tokamaks were summarized in a review in 2011 [3]. There the radially outward blob speed ranged over V_{rad} ~ 0.2–3 km s^{-1} and the poloidal blob size scale ranged over L_{pol} ~ 1–8 cm (FWHM), with a slight tendency for increased speed with increased blob size. The blob properties in the present paper are at the mid-to-low end of this velocity range and the mid-to-high end of this size range. Comparisons of the present results with some of the more recent measurements of blobs in tokamaks are summarized below (see also other papers in this special issue).

Blob sizes and velocities in the Alcator C-Mod SOL were measured in Ohmic plasmas using 2D GPI data with a blob tracking algorithm [6]. Blob sizes were in the range L_{pol} ~ L_{rad} ~ 0.7 cm, which is about ×4–6 smaller than those in NSTX, most likely due to the 10x larger toroidal field in C-Mod ($B = 5$ T). The radial blob velocities were V_{rad} ~ 0.1–0.4 km s^{-1} outward, similar to those in NSTX, while the poloidal blob velocities were V_{pol} ~ 0.1–0.4 km s^{-1} in the ion diamagnetic direction, somewhat lower than those in NSTX. Intermittent fluctuations were also studied in C-Mod using time series of GPI data [50], which showed large amplitude bursts with a fast rise and slow decay, which were characterized by a stochastic model.

Recent measurements of blobs were also done using GPI in the SOL of L-mode and H-mode plasmas in ASDEX Upgrade [22]. The average poloidal blob sizes were L_{pol} ~1.5 cm (FWHM) in Ohmic L-mode and H-mode, with a broad distribution of size scales in both cases. These sizes are about 3× smaller than those in NSTX (e.g. figure 6), most likely due to the 5× larger toroidal field in ASDEX ($B = 2.5$ T). The radial blob velocities in ASDEX were V_{rad} ~ 0.3 km s^{-1} in both Ohmic L-mode and H-mode, which is similar to the radial blob speeds seen in NSTX. There was a reversal of V_{pol} in Ohmic L-mode plasmas near the separatrix, and a similar blob detection rate in Ohmic and H-mode plasmas, both of which are similar to the NSTX results of figure 6. The radial blob velocities were also measured in ASDEX Upgrade in L-mode plasmas using a 1D Li-BES array [51], and these velocities decreased with increased blob size, similarly to the sheath-connected blob model and at least qualitatively similar to the results of figure 8(c) here.

Probe measurements of blobs in the SOL of NSTX [32] were generally similar to blobs seen by GPI, as discussed there. Probe measurements of SOL density fluctuations in MAST were recently compared with predictions of the ESEL turbulence code [52], and distributions of the measured radial size and perpendicular velocity of the filaments (i.e. blobs) appear to agree with those of the code. The fluctuations measured using probes in the SOL of TCV [53] were analyzed as a superposition of uncorrelated burst events, such that the average plasma density and fluctuations in the far SOL are due to the radial motion of blob-like structures. This statistical model appears to be at least qualitatively similar to the picture of blobs provided in the present paper.

10.5. Experimental directions

There are many possible directions for further experimental work on blobs in the SOL of tokamaks. Of fundamental diagnostic and physics importance would be the direct measurement of the 2D structure of the density and temperature within blobs, perhaps using the He I line ratio technique [54]. In addition, it would be valuable to have independent measurements of the SOL plasma flows and electrical currents on a blob timescale, e.g. using Mach probes and magnetic probes [55].

Although some good work has been done on the parallel correlation of SOL turbulence in tokamaks [29, 56], it would be highly interesting to image the entire 3D filamentary structure of blobs, e.g. to determine the effect of the X-point region and to examine how blobs connect to the divertor plate. This would most likely require multiple camera views and sophisticated image reconstruction. Finally, it might be possible to develop active blob control techniques to help manage heat

and particle removal at the tokamak wall; in particular, if the blob radial velocity can be increased, the SOL width should be increased. To this end, it would be useful to study 'seeded' blobs in the edge of a tokamak using highly localized edge sources, e.g. pulsed electron cyclotron heating or shallow pellets or dust.

Even without additional diagnostics, the analysis of blob structure and motion in the existing 2D imaging data can be significantly improved by allowing a variable blob fitting shape to better track the collisions, merging, and/or splitting of blobs. It is clear from viewing the movies of the present data [57] that there are many interesting features of blobs in the SOL of NSTX which have not been identified by the present analysis.

Acknowledgments

We thank for their contributions to this paper and this study in general: J W Ahn, S Banerjee, J A Boedo, O E Garcia, R W Gould, O Grulke, S I Krasheninnikov, S Kubota, R Maingi, T Munsat, S Sabbagh, Y Sechrest, J L Terry. This work was supported by #USDOE Contract DE-AC02-09CH11466 and DE-FG02-02ER54678. The digital data for this paper can be found at: http://arks.princeton.edu/ark:/88435/dsp01vx021h49j.

References

[1] Krasheninnikov S I 2001 *Phys. Lett.* A **283** 368
[2] Krasheninnikov S I *et al* 2008 *J. Plasma Phys.* **74** 679
[3] D'Ippolito D A *et al* 2011 *Phys. Plasmas* **18** 060501
[4] Ryutov D D 2006 *Phys. Plasmas* **13** 122307
[5] Walkden N R *et al* 2013 *Plasma Phys. Control. Fusion* **55** 105005
[6] Kube R *et al* 2013 *J. Nucl. Mater.* **438** S505
[7] Carralero D *et al* 2014 *Nucl. Fusion* **54** 102307
[8] Bisai N *et al* 2012 *Phys. Plasmas* **19** 052509
[9] Manz P *et al* 2013 *Phys. Plasmas* **20** 022308
[10] Russell D *et al* 2015 *Phys. Plasmas* **22** 092311
[11] Angus J R *et al* 2012 *Phys. Plasmas* **19** 082312
Angus J R *et al* 2014 *Phys. Plasmas* **21** 112504
[12] Halpern F D *et al* 2013 *Phys. Plasmas* **20** 092308
[13] Easy L *et al* 2014 *Phys. Plasma* **21** 122515
[14] Madsen J *et al* 2011 *Phys. Plasmas* **18** 112504
[15] Wiesenberger M *et al* 2014 *Phys. Plasmas* **21** 092301
[16] Manz P *et al* 2015 *Phys. Plasmas* **22** 022308
[17] Bodi K *et al* 2008 *Phys. Plasmas* **15** 102304
[18] Kendl A 2015 *Plasma Phys. Control. Fusion* **57** 045012
[19] Anderson J *et al* 2014 *Phys. Plasmas* **21** 122306
[20] Kube R 2015 *Phys. Plasmas* **22** 012502
[21] Garcia O E 2012 *Phys. Rev. Lett.* **108** 265001
[22] Fuchert G *et al* 2014 *Plasma Phys. Control. Fusion* **56** 125001
[23] Theiler C *et al* 2011 *Phys. Plasmas* **18** 055901
[24] Katz N *et al* 2008 *Phys. Rev. Lett.* **101** 015003
[25] Zweben S J *et al* 2004 *Nucl. Fusion* **44** 134
[26] Myra J R *et al* 2006 *Phys. Plasmas* **13** 092509
[27] Myra J R *et al* 2011 *Phys. Plasmas* **18** 012305
[28] Russell D A *et al* 2011 *Phys. Plasmas* **18** 022306
[29] Maqueda R *et al* 2010 *Nucl. Fusion* **50** 075002
[30] Maqueda R J *et al* 2011 *J. Nucl. Mater.* **415** S459
[31] Myra J R *et al* 2013 *Nucl. Fusion* **53** 073013
[32] Boedo J *et al* 2014 *Phys. Plasmas* **21** 042309
[33] Zweben S J *et al* 2015 *Nucl. Fusion* **55** 093035
[34] Zweben S J *et al* 2014 *Plasma Phys. Control. Fusion* **56** 095010
[35] Fundamenski W *et al* 2007 *Nucl. Fusion* **47** 417
[36] Eich T *et al* 2011 *Phys. Rev. Lett.* **107** 215001
[37] Ricci P *et al* 2013 *Phys. Plasmas* **20** 010702
[38] Myra J R *et al* 2015 *Phys. Plasmas* **22** 042516
[39] Boedo J *et al* 2001 *Phys. Plasmas* **8** 4826
[40] Simon P *et al* 2014 *Plasma Phys. Control. Fusion* **56** 095015
[41] Ionita C *et al* 2013 *Nucl. Fusion* **53** 043021
[42] Gray T K *et al* 2011 *J. Nucl. Mater.* **415** S360–4
[43] Mclean A G *et al* 2012 *Rev. Sci. Instrum.* **83** 053706
[44] Furno I *et al* 2011 *Phys. Plasmas* **53** 124016
[45] Jovanovic D *et al* 2008 *Phys. Plasmas* **15** 112305
[46] Boedo J A 2003 *Phys. Plasmas* **10** 1670
[47] Ouelette N T 2012 *C. R. Phys.* **13** 866
[48] Peacock T and Haller G 2013 *Phys. Today* **66** 41
[49] Zweben S J 1985 *Phys. Fluids* **28** 974
[50] Garcia O E *et al* 2013 *Phys. Plasmas* **20** 055901
[51] Birkenmeier G *et al* 2014 *Plasma Phys. Control. Fusion* **56** 075019
[52] Militello P *et al* 2013 *Plasma Phys. Control. Fusion* **55** 025005
[53] Garcia O E *et al* 2015 *Nucl. Fusion* **55** 062002
[54] Agostini M *et al* 2009 *Plasma Phys. Control. Fusion* **51** 105003
[55] Spolaore M *et al* 2015 *Phys. Plasmas* **22** 012310
[56] Grulke O *et al* 2014 *Nucl. Fusion* **54** 043012
[57] http://w3.pppl.gov/~szweben/PPCFblob/PPCFblob.html
http://arks.princeton.edu/ark:/88435/dsp01vx021h49j